



**VICTORIA UNIVERSITY**  
MELBOURNE AUSTRALIA

*Experimental and numerical studies of axially loaded square concrete-encased concrete-filled large-diameter steel tubular short columns*

This is the Published version of the following publication








Ci, Junchang, Kong, Lingxu, Ahmed, Mizan, Liang, Qing, Hamoda, Ahmed, Chen, Shicai and Wu, Chunyu (2022) Experimental and numerical studies of axially loaded square concrete-encased concrete-filled large-diameter steel tubular short columns. *Structural Concrete*, 23 (5). pp. 2748-2769. ISSN 1464-4177

The publisher's official version can be found at  
<https://onlinelibrary.wiley.com/doi/10.1002/suco.202100466>  
Note that access to this version may require subscription.

Downloaded from VU Research Repository <https://vuir.vu.edu.au/45097/>

## ARTICLE

# Experimental and numerical studies of axially loaded square concrete-encased concrete-filled large-diameter steel tubular short columns

Junchang Ci<sup>1</sup>  | Lingxu Kong<sup>2</sup>  | Mizan Ahmed<sup>3,4</sup>  | Qing Quan Liang<sup>5</sup>  | Ahmed Hamoda<sup>6</sup>  | Shicai Chen<sup>4</sup>  | Chunyu Wu<sup>1</sup> 

<sup>1</sup>College of Architecture and Civil Engineering, Beijing University of Technology, Beijing, China

<sup>2</sup>OCT Northern Investment Co. Ltd., Beijing, China

<sup>3</sup>School of Civil, Mining, and Environmental Engineering, University of Wollongong, Wollongong, New South Wales, Australia

<sup>4</sup>Department of Civil Engineering, Monash University, Clayton, Victoria, Australia

<sup>5</sup>College of Engineering and Science, Victoria University, Melbourne, Victoria, Australia

<sup>6</sup>Department of Civil Engineering, Kafrelsheikh University, Kafrelsheikh, Egypt

## Correspondence

Mizan Ahmed, School of Civil, Mining and Environmental Engineering, University of Wollongong, Wollongong, New South Wales 2522, Australia.  
Email: [mizan@uow.edu.au](mailto:mizan@uow.edu.au)

[Correction added on 15 April 2022, after first online publication: The missing CAUL funding statement has been added in this version.]

## Abstract

This article presents experimental and numerical studies on the axial compressive behavior of square concrete-encased concrete-filled steel tubular (CECFST) short columns composed of a circular inner steel tube. Tests on six full-scale short CECFST columns with the inner circular tube diameter varying from 320 to 500 mm were carried out to study the influences of sectional diameter and the tube thickness of circular CFST columns on their axial performance. A theoretical model is developed using fiber analysis method and validated against a large test database. The accuracy of various codified design models is evaluated and a simple model is proposed to calculate their ultimate strengths. Test results show that CECFST columns have improved load carrying capacity and can sustain large axial loads without significant strength degradation. In addition, increasing the thickness of the steel tube significantly improves the composite action of the steel and concrete of the inner CFST column, which increases the compressive strength of CECFST columns by 27.3%. However, the rate of increase in the compressive strength of the core concrete of the CFST column has been found to be higher for the column with a smaller local slenderness ratio. The ductility of CECFST columns is influenced by the concrete strength and the spacing of the stirrups. Furthermore, the design model suggested in this study can provide a better estimation than the codified design models.

## KEYWORDS

concrete-encased composite columns, fiber element modeling, inelastic buckling, nonlinear analysis, ultimate strengths

Discussion on this paper must be submitted within two months of the print publication. The discussion will then be published in print, along with the authors' closure, if any, approximately nine months after the print publication.

This is an open access article under the terms of the [Creative Commons Attribution](https://creativecommons.org/licenses/by/4.0/) License, which permits use, distribution and reproduction in any medium, provided the original work is properly cited.

© 2022 The Authors. *Structural Concrete* published by John Wiley & Sons Ltd on behalf of International Federation for Structural Concrete.

## 1 | INTRODUCTION

Concrete-filled steel tubular (CFST) columns offer improved strength, ductility, fire and seismic performance compared with traditional reinforced concrete columns; therefore are widely used in tall building structures, bridge piers and other composite constructions.<sup>1–5</sup> The steel tube acts as formwork during the construction and provides confinement to the core concrete.<sup>6,7</sup> However, the outer tube of CFST columns can be exposed to a harsh environment particularly in the marine environment which may cause significant corrosion to CFST columns, thus may affect their mechanical performance. A square concrete-encased concrete-filled steel tubular (CECFST) column as illustrated in Figure 1 is constructed by placing a circular steel tube into a square reinforced concrete column. Such composite columns were employed previously in composite tall buildings and bridges, such as in Huanggang Century Center and Lvjing Jiyuan building in Shenzhen.<sup>8</sup> The concrete encasement significantly improves the fire resistance, ease of connection to the beams, and the durability of CECFST columns in a corrosive environment when compared with concrete-filled steel tubular (CFST) columns.<sup>9</sup> Moreover, the presence of the inner steel tube markedly improves the ductility and strength performance of CECFST columns when compared with reinforced concrete columns. Despite their advantages over CFST columns and reinforced concrete columns, experimental and computational investigations into the behavior of CECFST columns with large diameter steel tubes have been relatively limited. Based on the literature, the maximum diameter of the inner tubes in the tested CECFST columns was 219 mm. However, CECFST columns with a large diameter of the inner tube are often used to carry heavy axial loads in composite construction. Therefore, further tests on short CECFST columns with a large-diameter inner tube should be carried out and accurate and robust computational and design methods for such composite columns should be developed accordingly.

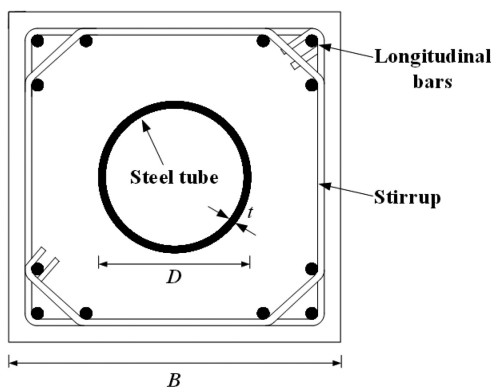


FIGURE 1 Cross-section of a CECFST column

A significant amount of research has been performed on conventional CFST columns to investigate the influences of different parameters on their performance under different loading conditions.<sup>10–19</sup> Previous studies show that circular tube provides more uniform confinement to the core concrete compared with rectangular section.<sup>14</sup> However, due to the ease of the connection to the beams, rectangular CFST columns are widely adopted in composite construction.<sup>20,21</sup> Considering this researchers also investigated various cross-sections of CFST columns such as elliptical section,<sup>22–24</sup> hexagonal section,<sup>25–28</sup> rounded CFST columns,<sup>29–32</sup> and octagonal section.<sup>33–36</sup> In combining the advantages of circular CFST columns and square outer sections, square CECFST columns were subsequently proposed. Investigations on the responses of CECFST short columns to axial compression were then performed by Chen,<sup>37</sup> Kang,<sup>38</sup> Liu,<sup>39</sup> Nie et al.,<sup>40</sup> and Liu et al.<sup>41</sup> Chen<sup>37</sup> examined the influences of the tube thickness on the axial behavior of short CECFST columns made of high-strength concrete. Test study showed that the peak loads of the specimens can be increased for the increase of the thickness of the tube. The maximum diameter of the inner tube in the tested columns was 133 mm. The significance of the diameter of the internal steel tube as well as the concrete strength on the axial performance of CECFST columns with the internal diameter of the steel varying from 140 to 180 mm was examined by Liu et al.<sup>41</sup> The peak compressive loads of the tested columns were found to be improved for the increase in the strength of concrete or the diameter of the steel tube. Furthermore, Ji et al.<sup>42</sup> and Han et al.<sup>43</sup> studied the cyclic behavior of CECFST columns. They reported that the bending capacities of tested CECFST columns were significantly higher than those of traditional reinforced concrete columns. Recently, Ma et al.<sup>44</sup> tested CECFST stub columns subjected to biaxial loading. The ductility of the tested columns was affected by the loading eccentricity and end moment ratio. Zhou and Han<sup>45</sup> also performed a test to investigate the fire performance of the joints between the reinforced concrete beam and CECFST columns. The failure of the test specimens was similar to the beam failure and no fire-induced spalling could be observed in the outer RC component due to the utilization of lower strength concrete. The inner tube also protected the spalling of the high-strength core concrete.

The behavior of CECFST short columns loaded eccentrically to failure was ascertained by Guo et al.<sup>46–47</sup> and An et al.<sup>48</sup> experimentally. It was reported that the ductility and ultimate strength of CECFST columns were markedly reduced by increasing the eccentricity ratio. The numerical models of finite element (FE) were created by Han and An<sup>9</sup> and An and Han<sup>49</sup> using ABAQUS to investigate the responses of CECFST columns loaded either

axially or eccentrically. Good agreement between the test and numerical results can be observed. However, the development of such an FE model is tedious, time-consuming, and often confronts the problem associated with convergence issues. Therefore, the fiber-based numerical model is widely used nowadays as an economical and computationally advanced scheme compared with the traditional FE model to investigate composite structures.<sup>50–56</sup>

This article presents an experimental program carried out to study the structural responses of full-scale square CECFST short columns loaded axially and developed a theoretical model based on the fiber analysis for the performance prediction of CECFST columns. The experimental program is described first. This is followed by the formulation and validation of the fiber-based theoretical model. A parametric study on the responses of CECFST columns using the computer modeling program written is then given. The accuracy of various codified design methods and the proposed design equation for designing square CECFST short columns are examined. Finally, conclusions drawn from this research are summarized.

## 2 | RESEARCH SIGNIFICANCE

The literature review shows that investigations on CECFST columns with large diameters are missing and a fiber-analysis technique has not been developed for determining the performance of CECFST columns. Furthermore, there are no design guidelines available for designing such a column in the existing design codes Eurocode 4,<sup>57</sup> ACI 318-14,<sup>58</sup> and AIJ.<sup>59</sup> However, CECS 188-2019<sup>60</sup> provides design guidelines for CECFST columns. The applicability of existing design codes for reinforced concrete and CFST columns to CECFST columns has not been investigated. Thus, this study fills these knowledge gaps by testing large-diameter short CECFST columns with a maximum outer cross-section of 600 × 600 mm. The diameter of the inner circular tube varied from 320 to 500 mm which exceeded the maximum diameter of the inner circular tube of existing CECFST columns reported in the literature. The accuracy of the design specifications in various design codes is evaluated and a more accurate design model is proposed in this study.

## 3 | EXPERIMENTAL PROGRAM

### 3.1 | Test specimens

A total of six square large-scale CECFST stub columns with different cross-sectional sizes and material properties was tested under axial compression. The cross-section of a CECFST column is illustrated in Figure 1, in

which  $B$  denotes the cross-sectional width of the column;  $D$  stands for the diameter of the inner steel tube and  $t$  is its thickness. According to the section size of the column, the column specimens were grouped into three groups, namely G1, G2, and G3. Each group consisted of two specimens, and the variation parameter was the tube thickness. In the selection of the diameter and thickness of the inner circular tube, the slenderness limits of the steel tube specified by Eurocode 4,<sup>57</sup> AS 5100,<sup>61</sup> ACI 318-19,<sup>58</sup> and AISC 360-16<sup>62</sup> were considered. Eurocode 4<sup>57</sup> specifies a local slenderness limit  $\frac{D}{t} \left( \frac{f_{sy}}{235} \right) \leq 90$  while AS 5100,<sup>61</sup> ACI 318-19,<sup>58</sup> and AISC 360-16<sup>62</sup> specify the local slenderness limit of the outer tube of the CFST column as  $\frac{D}{t} \left( \frac{f_{sy}}{235} \right) \leq 82$ ,  $\frac{D}{t} \sqrt{\frac{f_{sy}}{E_s}} \leq \sqrt{8}$ , and  $\frac{D}{t} \left( \frac{f_{sy}}{E_s} \right) \leq 0.31$ , respectively. Furthermore, the maximum concrete compressive strength specified by Eurocode 4,<sup>57</sup> AS 5100,<sup>61</sup> ACI 318-19,<sup>58</sup> and AISC 360-16<sup>62</sup> was as 20–50 MPa, 25–65 MPa,  $\geq 17.2$  MPa, and 21–70 MPa, respectively. Furthermore, to suppress the overall buckling, the height ( $L$ ) of all column specimens was chosen to be three times the width ( $B$ ) of their cross-sections. Based on the aforementioned design specifications and markedly available steel plates, preliminary theoretical analysis was undertaken to calculate the theoretical ultimate strengths of CECFST tested columns to ensure that all specimens are within the limits of maximum height and loading capacity of the testing machine available.

The material properties, and geometric and reinforcement details of the column specimens are provided in Table 1, where  $f_{co}$  represents the cube compressive strength of the concrete outside the inner tube;  $f_{ci}$  is the cube strength of the core concrete filled in the inner tube;  $s$  is the spacing of stirrups;  $\Phi_l$  and  $\Phi_p$  are the diameters of the longitudinal reinforcement and stirrups, respectively.

The formworks of CECFST columns are shown in Figure 2. In preparing the specimens, the steel plates with different thicknesses were first rolled and welded to form the inner circular steel tubes as illustrated in Figure 2a. The longitudinal reinforcing bars and stirrups were then placed outside the tube; the formwork was erected, and finally, the concrete was poured. As discussed by Zhou and Han,<sup>45</sup> to achieve improved seismic performance, the load-carrying capacity of the inner CFST column is usually designed to be higher than that of the outer RC columns. This can be achieved by using higher-strength concrete for the core section than that of the concrete for the RC component. Similarly, in this study, the strength of concrete for the inner tube was designed to be higher than the outer concrete. Consequently, the steel tube was filled with concrete first, and then concrete with a different mix was used to fill the

TABLE 1 Details of the tested specimens

Group	Specimen	$L$ (mm)	$B \times B$ (mm)	$D \times t$ (mm)	$f'_{co}$ (MPa)	$f'_{ci}$ (MPa)	Longitudinal bar	Stirrup	Ultimate load $P_{u,test}$ (kN)
G1	CEC1-1	1200	400 × 400	320 × 6	35.6	47.2	12Φ12	8@150	7437
	CEC1-2	1200	400 × 400	320 × 10	35.6	47.2	12Φ12	8@150	9468
G2	CEC2-1	1500	500 × 500	400 × 8	35.6	47.2	12Φ16	8@120	12,578
	CEC2-2	1500	500 × 500	400 × 12	35.6	47.2	12Φ16	8@120	15,021
G3	CEC3-1	1800	600 × 600	500 × 10	35.6	47.2	12Φ18	10@200	18,318
	CEC3-2	1800	600 × 600	500 × 16	35.6	47.2	12Φ18	10@200	22,880

FIGURE 2 Fabrication of CECFST column specimens:

(a) fabrication of steel tubes,  
(b) reinforcement, and  
(c) casting concrete

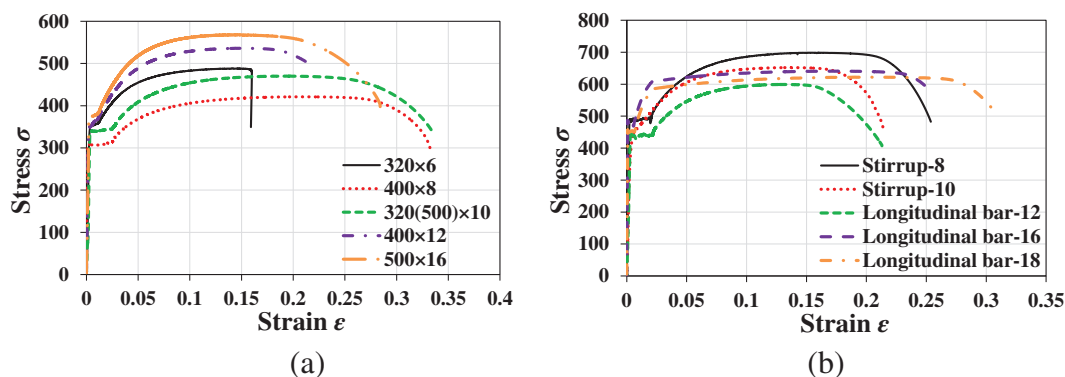


FIGURE 3 Measured stress-strain curves of tensile coupon specimens: (a) steel tubes, and (b) longitudinal bar and stirrups

space between the formwork and the steel tube. To prevent the failure of specimen ends, both ends of each specimen were embedded with steel mesh.

### 3.2 | Material properties

To obtain the material properties of steel tubes, three standard tensile coupons were cut from each steel tube. Tensile tests were undertaken according to Chinese standard GB/T 228.1-2010.<sup>63</sup> Similarly, the properties of reinforcements were determined by means of conducting tensile tests on longitudinal bars and stirrups. The

measured stress-strain relationships of typical tensile coupons are shown in Figure 3. Table 2 presents the measured mechanical properties of steel materials, including yield strength  $f_{sy}$ , modulus of elasticity  $E_s$ , tensile strength  $f_u$  and ultimate tensile strain  $\epsilon_u$ , expressed as the average value  $\pm$  SD of three test coupons. Ready-mixed concrete was used to construct all column specimens. To measure the strength of unconfined concrete, three concrete cubes ( $150 \times 150 \times 150$  mm) were made for each concrete grade. Compressive tests were carried out on concrete cubes at least 28 days after casting to determine their compressive strengths ( $f_{cu}$ ) in accordance with Chinese standards GB/T 50081-2019.<sup>64</sup> The average



TABLE 2 Material properties of steel tubes obtained from tensile coupon tests

Steel type	No.	Geometry dimension of steel	$f_{sy}$ (MPa)	$E_s$ (GPa)	$f_u$ (MPa)	$\varepsilon_u$
Steel tube $D \times t$ (mm)	1	320 × 6	358.7 ± 3.7	193.2 ± 6.6	491.9 ± 2.4	0.13 ± 0.03
	2	400 × 8	308.3 ± 4.2	204.2 ± 2.1	421.1 ± 1.8	0.21 ± 0.11
	3	320 × 10	346.7 ± 2.2	200.4 ± 0.9	470.0 ± 1.5	0.21 ± 0.04
	4	500 × 10	346.7 ± 2.2	200.4 ± 0.9	470.0 ± 1.5	0.21 ± 0.04
	5	400 × 12	371.5 ± 2.1	202.4 ± 1.1	506.4 ± 3.4	0.16 ± 0.09
	6	500 × 16	380.4 ± 3.9	203.5 ± 2.4	567.8 ± 1.6	0.15 ± 0.19
Steel bar	7	Stirrup- Φ8	483.7 ± 7.1	196.1 ± 9.2	701.7 ± 2.1	0.15 ± 0.09
	8	Stirrup- Φ10	434.7 ± 1.2	198.4 ± 2.9	663.7 ± 3.3	0.25 ± 0.03
	9	Longitudinal bar- Φ12	432.0 ± 3.0	202.5 ± 1.4	599.1 ± 4.1	0.14 ± 0.09
	10	Longitudinal bar- Φ16	470.1 ± 1.7	200.3 ± 1.7	642.2 ± 1.5	0.16 ± 0.04
	11	Longitudinal bar- Φ18	442.7 ± 3.4	198.2 ± 3.1	627.7 ± 3.1	0.19 ± 0.12

compressive strength of the concrete used to fill the steel tube and outside the steel tube was measured as 35.6 and 47.2 MPa, respectively.

### 3.3 | Test setup and instrumentations

All column specimens were tested under compression using the 112,000 kN large-scale multifunctional structure testing system in the Key Laboratory of Beijing University of Technology, China. The test set-up of the column specimen and instruments are shown in Figure 4. The load was directly applied to the column specimen by the downward movement of the loading ram at the upper end of the column specimen, which was pulled by the four electro-hydraulic servo loading systems of the loading machine. Four 600 mm range precise draw-wire displacement sensors were installed between the base plate and the loading plate to measure the end shortening of the specimen under axial loading.

To measure the strain distribution in the components of a column specimen, strain gauges were attached to each component at different positions (steel tube, longitudinal bar, stirrup, outer concrete, and acrylic rod) at the mid-height cross-section. The numbers and locations of strain gauges and displacement sensors are schematically illustrated in Figure 5. To distinguish the location of strain gauges, each strain gauge was numbered. Take 'TZ' as an example: (I) 'T' indicates that the strain gauge was pasted on the outer surface of the steel tube ('L': 'longitudinal reinforcement', 'A': 'acrylic rod', 'P': 'stirrup' and 'C': 'concrete'); (II) 'Z' represents the longitudinal strain measured in the column height direction ('H':

horizontal direction). To measure the strain inside the concrete, the strain gauge was pasted on a 4 × 4 mm acrylic rod and fixed at the mid-length of the column along the length direction through the metal wire. To increase the adhesion with the concrete, sandpaper was used to grind the rod on each side of the bar and cut the groove.

The loading method specified in Chinese standard GB/T 50152-2012<sup>65</sup> was adopted in this test. To ensure that the uniform compression was applied to the end of the column specimen, both ends of the column specimen were smoothed with high-strength gypsum, and the load-displacement double control method was adopted for loading. The column specimen was preloaded to 5% of its estimated ultimate strength to ensure the correctness of the connection of instruments

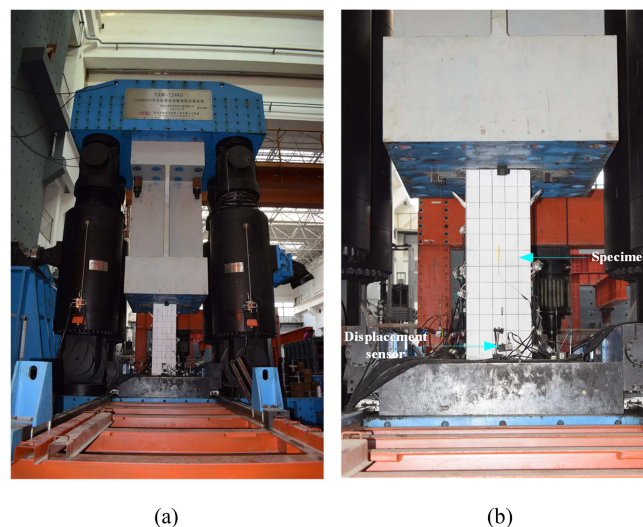
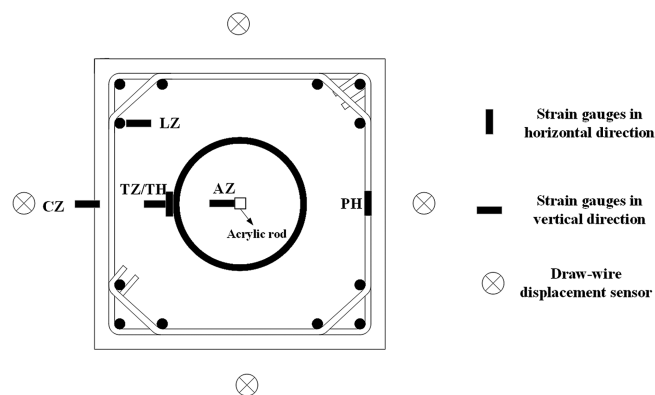


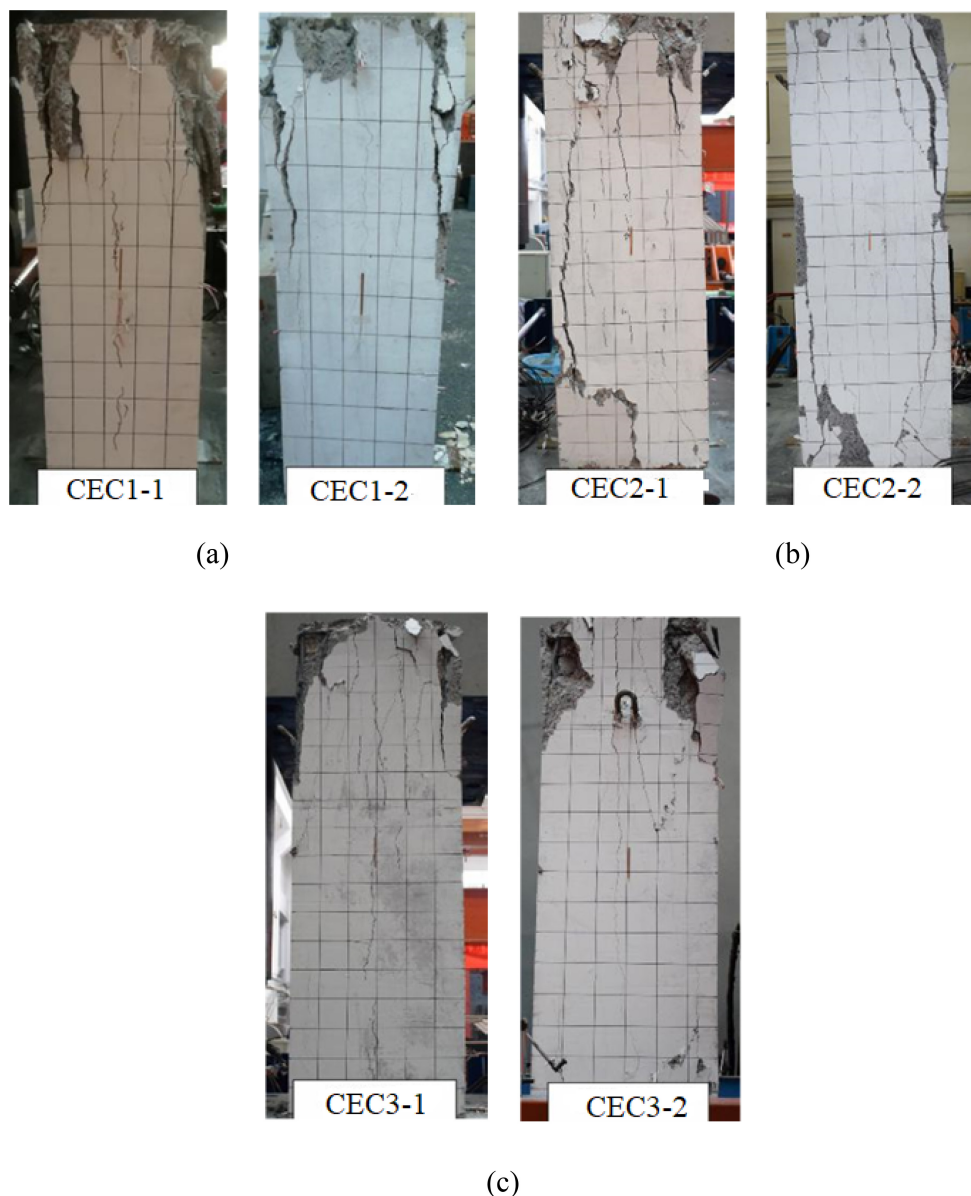
FIGURE 4 Test setup of the column specimen



**FIGURE 5** Arrangement of strain gauges and displacement sensors in the column specimen

and the accuracy of data collections. This also eliminated any possible gap between the specimen and the loading plate and any possible initial bending effect of the specimens. Each column was initially tested under the force control method with a loading rate of 6–17 kN/s. When the applied load reached 80 ~ 90% of the estimated ultimate strength of the column, the displacement control method was used, which ensured that the complete axial load-strain curve of the column was obtained. According to the size of the specimen, the displacement loading rate was slightly different. When the axial load decreased to 60% of the column ultimate load or the concrete spalled or crushed, it was assumed that the specimen failed.

**FIGURE 6** Failure modes of tested column specimens: (a) Group 1, (b) Group 2, and (c) Group 3



## 4 | TEST RESULTS AND DISCUSSIONS

### 4.1 | Failure modes

Figure 6 presents the failure modes of all column specimens. It can be seen that all specimens generally failed by the crushing of the concrete outside the steel tube with obvious deformations of stirrups and longitudinal bars in the vicinity of the crushed concrete. However, slight differences between the failure modes of three groups of specimens with different sizes were discovered. The failure pattern of the first group of specimens was mainly the cracking and spalling of the concrete outside the steel tube in the middle and upper parts of the column. The failure of the second group of specimens was characterized by the oblique cracks of the cover concrete at both ends of the column, which extended to the middle of the column where the cover concrete bulged and fell off. The third group of specimens failed by the crushing of the concrete located outside the steel tube at the upper end of the column. It was observed that the inner CFST columns of the tested specimens did not fail, which reflects the excellent capacity of CECFST columns.

### 4.2 | The ultimate strengths of stub columns

The experimentally measured load-axial strain curves of the tested column specimens are presented in Figure 7, where the strain was calculated as the ratio of the end

shortening ( $\delta$ ) to the column length ( $L$ ). At the initial stage of loading, the axial load-strain curves of all specimens were straight lines, which indicate that all parts of the specimen remained elastic at this stage. When the axial load reached 75–90% of the column ultimate load, the slope of the curve began to decrease, and the specimen entered the elastic-plastic stage. At this stage, the concrete outside the steel tube cracked. It is worth noting that before the ultimate load was reached, no obvious failure occurred in all specimens. The spalling of the cover concrete occurred after the ultimate loads of the columns have attained. In the later stage of loading, although the concrete located outside the steel tube was seriously crushed, all the specimens showed excellent residual strengths, which were about 85 ~ 95% of their peak loads. This indicates that CECFST columns have good ductility. The utilization of the CFST column was found to increase the ultimate strength of the CECFST column, as shown in Table 3. It should be noted that in the superposition method, the concrete cube strengths were converted to the cylindrical strengths using the following formula proposed by L'Hermite<sup>66</sup> and the strength of cover concrete was reduced by a strength reduction factor of 0.85 to consider the column size effects, as suggested by ACI 316-19.<sup>58</sup> The increase in the ultimate strength calculated varied from 6% to 12%. However, the insignificant increase in the ultimate load of Column CEC1-1 was caused by the fact that the concrete strength as the average concrete cylindrical strength was used to calculate the ultimate loads of the columns.

The measured ultimate loads of the specimens are listed in Table 1. From Table 1 and Figure 7, it can be

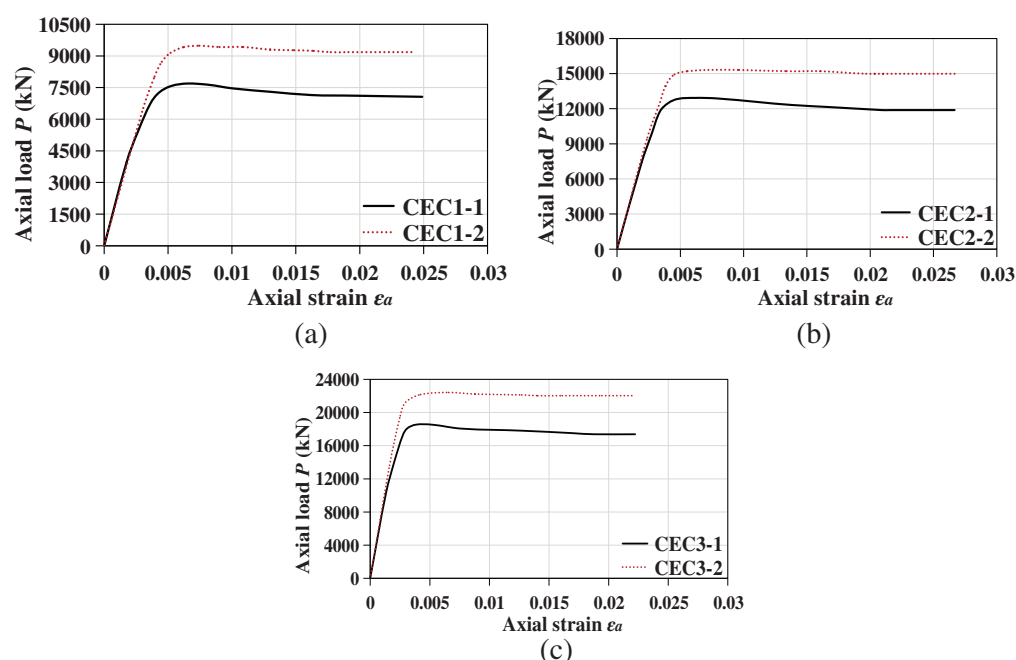


FIGURE 7 Measured axial load-strain curves of tested column specimens: (a) Group 1, (b) Group 2, and (c) Group 3

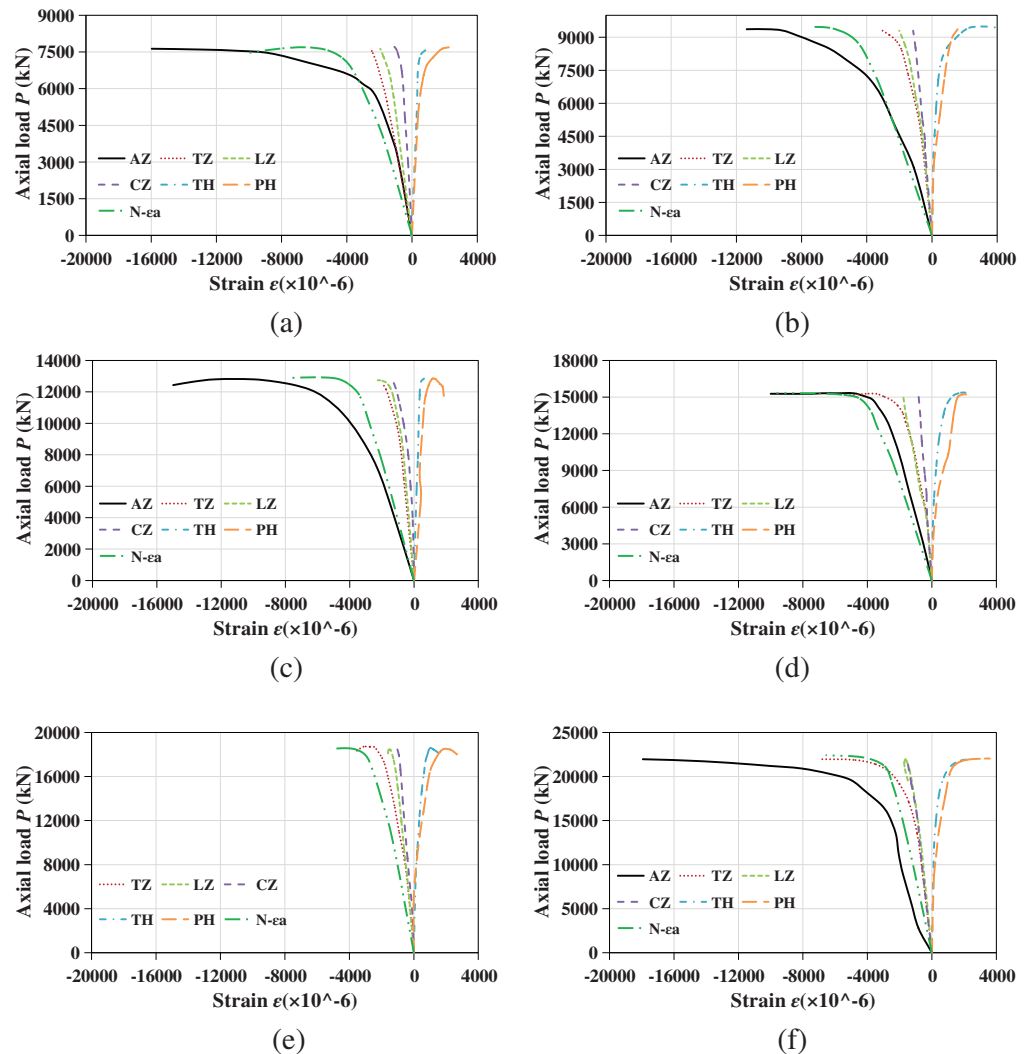


TABLE 3 Improvement of the compressive strength of core concrete of CECFST columns

Group	Specimen	$f'_{co}$ (MPa)	$f'_{ci}$ (MPa)	Ultimate load $P_{u, test}$ (kN)	Superposition load (kN)	Increase in the ultimate strength (kN)	$f'_{ce}/f'_c$
G1	CEC1-1	35.6	47.2	7437	7341	96	1.03
	CEC1-2	35.6	47.2	9468	8445	1023	1.37
G2	CEC2-1	35.6	47.2	12,578	11,444	1134	1.25
	CEC2-2	35.6	47.2	15,021	13,662	1359	1.31
G3	CEC3-1	35.6	47.2	18,318	17,202	1116	1.16
	CEC3-2	35.6	47.2	22,880	20,849	2031	1.30

FIGURE 8 Measured axial load versus axial and hoop strain curves of tested column specimens:

(a) specimen CEC1-1,  
(b) specimen CEC1-2,  
(c) specimen CEC2-1,  
(d) specimen CEC2-2,  
(e) specimen CEC3-1, and (f)  
specimen CEC3-2



seen that the steel tube thickness has a great impact on the performance of CECFST columns. For Group G1, the thickness of steel tubes was increased from 6 to 10 mm which resulted in an increase in the column ultimate strength by 27.3%. Similarly, for Groups G2 and G3, the increase in the ultimate strengths due to an increase in the tube thickness was determined as 19.2% and 24.9%, respectively. Increasing the thickness of the steel tube

increases the steel area, thus increasing the lateral pressure to the confined concrete. Therefore, the peak compressive loads of such columns can be improved by increasing the steel ratio of the columns. The effect of the thickness of the steel tube on the compressive strength of core concrete was investigated and calculated using the superposition method. From Table 3, it is seen that increasing the thickness of the steel tube increased the

compressive strength of core concrete of CECFST columns. However, the rate of increase was found to be higher for the column with a smaller section slenderness ratio. The local slenderness ratios for Columns CEC1-1, CEC2-1, and CEC3-1 were calculated as 81, 66, and 74, respectively according to Eurocode 4, whereas the local slenderness ratios for Columns CEC1-2, CEC2-2, and CEC3-2 were calculated as 47, 53, and 51, respectively. The increase in the compressive strength of the core concrete of Columns CEC1-2, CEC2-2 and CEC3-2 was calculated as 32%, 5%, and 12% higher than the compressive strength of the core concrete of Columns CEC1-1, CEC2-1, and CEC3-1, respectively. It should be noted that due to the insignificant increase in the ultimate load of Column CEC1-1 calculated according to the superposition method discussed earlier, the rate of increase in the compressive strength of the core concrete of Column CEC1-2 may be overestimated compared with that of the Column CEC1-1.

### 4.3 | Strain distributions

The variations of strain in different parts of the tested specimens against the axial load are demonstrated in Figure 8. The negative side represents the axial load-longitudinal strain relationships, while the positive side shows the axial load-hoop strain relationships. Since some of the strain gauges were damaged by the large deformation and concrete crushing in the inelastic range, only recorded strains by strain gauges before damaging are presented in Figure 8. Due to the failure of the strain gauge on the acrylic bar in specimen CEC2-1, it is not shown in the figure. By analyzing the load-strain curves, it can be found that at the elastic stage, with increasing the load, the longitudinal strain and hoop strain show a linear increasing trend. The strains of steel tube, concrete, longitudinal bar, and stirrup are all small before the peak load, which indicates that these parts have just started or have not entered the inelastic stage. However, upon reaching the ultimate load, the strain increased remarkably owing to the rapid expansion of outer concrete.

## 5 | THEORETICAL MODEL

### 5.1 | General

A theoretical model employing the fiber analysis technique is developed to simulate the nonlinear performance of CECFST columns loaded axially. Such a numerical

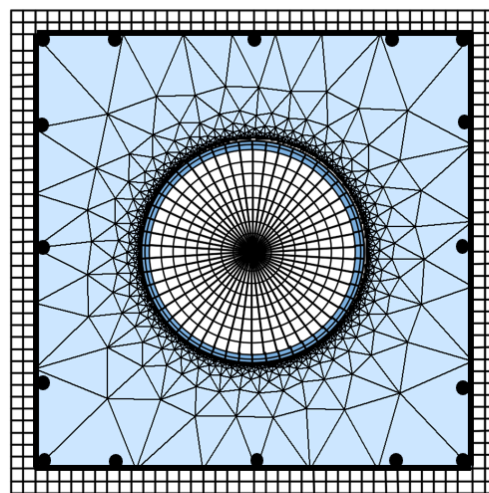


**FIGURE 9** Typical fiber discretization of the cross-section of a CECFST column

scheme has computational efficiency when compared with traditional finite element software.<sup>55,67–68</sup> The composite section of a CECFST column is divided into fibers with small areas as illustrated in Figure 9. The axial stress of each fiber is computed from its corresponding axial strain by employing the uniaxial stress-strain relationships of materials. The axial load is calculated as the stress resultant over the entire cross-section.

### 5.2 | Constitutive laws of structural steel and reinforcement

The stress-strain relationships of structural steel adopted for the steel tube are illustrated in Figure 10a. The material model considers the influence of biaxial stresses on the steel tube due to the effective confinement effects by reducing the yield stress by a factor of 0.9. The expressions suggested by Liang<sup>50</sup> are used to calculate the stresses from  $0.9 \varepsilon_{sy}$  ( $\varepsilon_{sy}$  denotes the yield strain) to the strain  $\varepsilon_{st}$  at the onset of strain-hardening, which is specified as 0.005. The formulas given by Mander<sup>69</sup> are adopted to the stresses from  $\varepsilon_{st}$  to the ultimate strain  $\varepsilon_{su}$  which is prescribed as 0.2.

Longitudinal reinforcing bars in a CECFST short column loaded concentrically may buckle after the cover concrete has crushed as depicted in Figure 6. The buckling of longitudinal reinforcements considerably reduces the strength of CECFST columns so that it must be included in the nonlinear simulation of such composite columns. Longitudinal reinforcing bars are tied by transverse stirrups with a small spacing, which usually prevent them from elastic buckling. Therefore, only inelastic

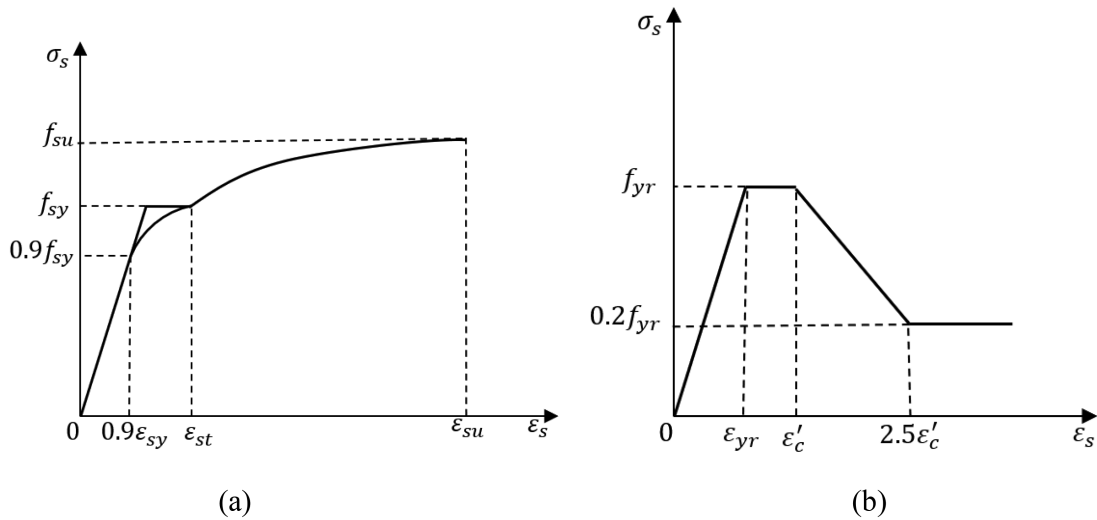


FIGURE 10 Typical stress-strain curves for (a) structural steel and (b) longitudinal reinforcing bars

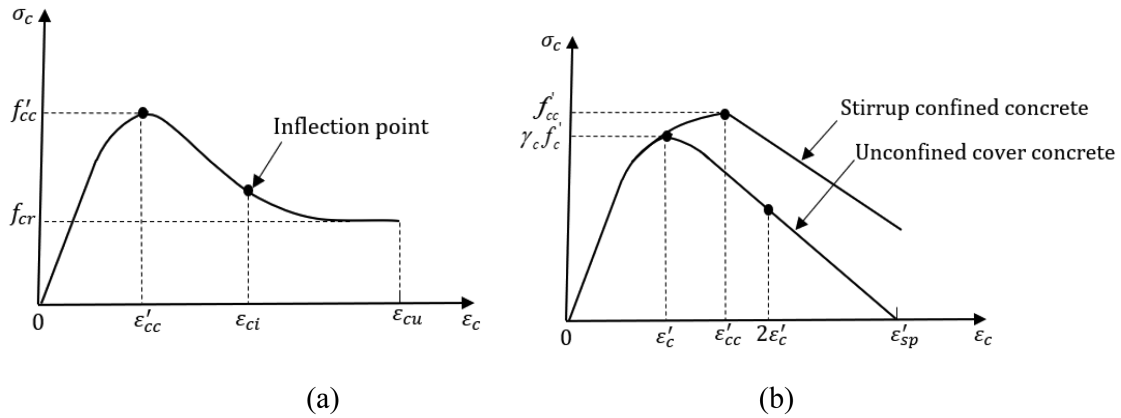


FIGURE 11 Idealized stress-strain curves for concrete: (a) core concrete and (b) unconfined and stirrup confined concrete

buckling of longitudinal reinforcements is incorporated in the present numerical model by means of modifying the stress-strain model of rebars in compression. The stress-strain relationships for longitudinal rebars in axial compression shown in Figure 10b account for the inelastic buckling of rebars with a length taken as the spacing of stirrups. The model assumes that the longitudinal rebar starts undergoing inelastic buckling once the cover concrete is crushed and its strength linearly reduces to 20% of its yield strength from the concrete strain  $\epsilon'_c$  to  $2.5\epsilon'_c$ , and thereafter remains constant as illustrated in Figure 10b.<sup>70</sup>

### 5.3 | Constitutive laws of concrete

The concrete in a CECFST column is divided into the core concrete that is confined by the steel tube, stirrup confined concrete, and unconfined cover concrete. The

following sections present the stress-strain relationships of concrete used for different regions.

#### 5.3.1 | Stress-strain relationships for the core concrete

Figure 11a illustrates the stress-strain relationships of the core concrete that is confined by the circular steel tube. The ascending part is described by the equation suggested by Mander et al.<sup>71</sup> as follows:

$$\sigma_c = \frac{f'_{cc}(\epsilon_c/\epsilon'_{cc})^\lambda}{\lambda + (\epsilon_c/\epsilon'_{cc})^\lambda - 1} \quad (1)$$

$$\lambda = \frac{\epsilon'_{cc}}{\epsilon'_{cc} - (f'_{cc}/E_c)} \quad (2)$$

where  $\sigma_c$  and  $\varepsilon_c$  are the longitudinal stress and strain, respectively;  $E_c$  denotes Young's modulus of concrete estimated by  $E_c = 4400(\gamma_c f'_c)^{0.5}$ , in which  $\gamma_c$  stands for the strength reduction factor considering the size effect provided by Liang and Fragomeni<sup>72</sup> for the filled concrete confined by a circular steel tube;  $f'_{cc}$  is the compressive strength of confined concrete;  $\varepsilon'_{cc}$  refers to the strain at  $f'_{cc}$ .

The maximum strength and its strain of confined concrete are expressed by the following equations of Mander et al.<sup>33</sup>

$$f'_{cc} = \left(1 + \frac{4.1f_{rp}}{\gamma_c f'_c}\right) \gamma_c f'_c \quad (3)$$

$$\varepsilon'_{cc} = \left(1 + \frac{20.5f_{rp}}{\gamma_c f'_c}\right) \varepsilon'_c \quad (4)$$

where  $f_{rp}$  represents the lateral stress provided by the circular steel tube to the core concrete;  $\varepsilon'_c$  is the strain at  $\gamma_c f'_c$  and is given by De Nicolo et al.<sup>73</sup> as

$$\varepsilon'_c = \sqrt{[0.626(\gamma_c f'_c) - 4.33] \times 10^{-7} + 0.00076} \quad (5)$$

The lateral pressure model for concrete in circular CFST columns developed by Liang and Fragomeni<sup>72</sup> is used to estimate  $f_{rp}$  on the core concrete in CECFST columns, which is written as:

$$f_{rp} = \begin{cases} 0.7(v_e - v_s) \frac{2t}{D-2t} f_{sy} & \text{for } \frac{D}{t} \leq 47 \\ \left(0.006241 - 0.0000357 \frac{D}{t}\right) f_{sy} & \text{for } 47 < \frac{D}{t} \leq 150 \end{cases} \quad (6)$$

in which  $f_{sy}$  denotes the yield stress of the structural steel material;  $v_s$  stands for Poisson's ratio of the hollow steel tube, specified as 0.5; and  $v_e$  is Poisson's ratio of the steel tube that is filled with concrete proposed by Tang et al.<sup>74</sup>

The descending part of the stress-strain curve of concrete was originally proposed by Lim and Ozbakkaloglu<sup>75</sup> as:

$$\sigma_c = f'_{cc} - \frac{f'_{cc} - f_{cr}}{\left[\left(\frac{\varepsilon_c - \varepsilon'_{cc}}{\varepsilon_{ci} - \varepsilon'_{cc}}\right)^{-2} + 1\right]} \quad (7)$$

in which  $f_{cr}$  is the residual concrete compressive strength, and  $\varepsilon_{ci}$  is the strain that defines the inflection point, given by Lim and Ozbakkaloglu<sup>75</sup> as:

$$\varepsilon_{ci} = 2.8\varepsilon'_{cc} \left(\gamma_c f'_c\right)^{-0.12} \left(\frac{f_{cr}}{f'_{cc}}\right) + 10\varepsilon'_{cc} \left(\gamma_c f'_c\right)^{-0.47} \left(1 - \frac{f_{cr}}{f'_{cc}}\right) \quad (8)$$

The concrete residual strength ( $f_{cr}$ ) is calculated by  $f_{cr} = \beta_c f'_{cc}$ , in which  $\beta_c$  is strength degradation parameter provided by Liang and Fragomeni<sup>72</sup> as

$$\beta_c = \begin{cases} 1.0 & \text{for } 21.7 \leq D/t \leq 40 \\ 0.0000339(D/t)^2 - 0.010085(D/t) + 1.3491 & \text{for } 40 < D/t \leq 150 \end{cases} \quad (9)$$

### 5.3.2 | Stress-strain relationships for the outer concrete

The stress-strain constitutive laws for unconfined concrete presented by Mander et al.<sup>71</sup> as illustrated in Figure 11b are adopted for the cover concrete in a CECFST column. The maximum compressive strength of unconfined concrete is calculated as  $f'_{cc} = \gamma_c f'_{co}$  where  $\gamma_c = 0.85$  to consider the size effects.<sup>76</sup> The descending part of the curve from the onset of the transition point where  $\varepsilon_c > 2\varepsilon'_c$  is assumed to be a straight line up to the spalling strain ( $\varepsilon'_{sp}$ ) taken as 0.006 based on the test results.<sup>77</sup>

Equation (1) is employed to describe the ascending part of the stress-strain curve for concrete confined by stirrups. The maximum compressive strength and the corresponding strain of concrete confined by stirrups are calculated using Equations (10,11) suggested by Wang et al.<sup>78</sup>

$$f'_{cc} = \gamma_c f'_c [1 + 1.73(\theta)^{0.55}] \leq 1.5f'_c \quad (10)$$

$$\varepsilon'_{cc} = \varepsilon'_c [1 + 142(\theta)^{1.55}] \leq 0.01 \quad (11)$$

where  $\theta$  is the confinement index of stirrup confined concrete can be determined as:<sup>78</sup>

$$\theta = \frac{f_{le}}{\gamma_c f'_c} \quad (12)$$

where  $f_{le}$  is the effective lateral confinement stress of stirrup calculated as  $f_{le} = k_e f_l$ , where  $f_l$  is expressed as.

$$f_l = k_e \rho_w \sigma_s \quad (13)$$

$$k_e = (0.04n + 0.97) \times \left(1 - \frac{1}{n}\right) \times \left(1 - 0.5 \frac{s}{B}\right) \quad (14)$$



in which  $\rho_w$  is the volumetric ratio of stirrups;  $s$  is the spacing of stirrups;  $n$  is the number of stirrups along the length of the column; and  $\sigma_s$  is the tensile stress in the stirrups when the confined concrete reaches the compressive strength, which can be determined as:<sup>78</sup>

$$\sigma_s = 12.29 \frac{k_e E_s \rho_w}{\gamma_c f'_c} + 180 \leq f_{sy} \quad (15)$$

in which  $E_s$  and  $f_{sy}$  are Young's modulus and yield stress of stirrup, respectively.

The descending part of the stress-strain curves of concrete confined by stirrups is assumed to be a straight line<sup>9</sup> and is represented by:

$$\sigma_c = f'_{cc} - E_{det} (\epsilon_c - \epsilon'_{cc}) \quad (16)$$

in which  $E_{det}$  is the rate of deterioration between the maximum stress and 85% of the maximum stress calculated as

$$E_{det} = \frac{0.15 f'_{cc}}{\epsilon'_{0.85} - \epsilon'_{cc}} \quad (17)$$

$$\epsilon'_{0.85} = \epsilon'_{cc} + 0.225 \rho_w \sqrt{\frac{B}{s}} \quad (18)$$

## 6 | VERIFICATION OF THE THEORETICAL MODEL

The verification of the accuracy of the theoretical model is performed by comparisons of the predicted strengths and the load-axial strain ( $P-\epsilon$ ) curves of CECFST columns with the test results reported in this study as well as available in the literature. The concrete cube strengths were converted to the cylindrical strengths using the following formula proposed by L'Hermite<sup>66</sup>:

$$f'_c = \left[ 0.76 + 0.2 \log_{10} \left( \frac{f_{cu}}{19.6} \right) \right] f_{cu} \quad (19)$$

The comparisons of the ultimate loads of CECFST columns under investigation are presented in Table 4 where it can be seen that the theoretical model can reasonably yield the test ultimate strengths of such columns. The mean of the predicted-to-experimental ultimate strength is 0.96. The predicted  $P-\epsilon$  curves employing the theoretical model are presented in Figures 12 and 13.

A reasonable match between the test results and the theoretical predictions can be observed.

## 7 | PARAMETER STUDY

The theoretical model was employed to examine the influences of importance column parameters on the performance of CECFST columns loaded axially. The details of the reference column were  $B=700$  mm,  $D \times t=500 \times 10$  mm,  $f_{sy}=350$  MPa,  $f_{syr}=f_{sys}=400$  MPa, and  $f'_{co}=f'_{ci}=50$  MPa, the number of the longitudinal bars = 12 mm, the diameter of the longitudinal rebars = 20 mm, the diameter of the stirrup = 10 mm, space  $s=200$  mm, concrete cover = 40 mm and  $E_s=200$  GPa.

### 7.1 | Influences of the diameter-to-thickness ( $D/t$ ) ratio

The  $D/t$  ratio of the columns varied from 30 to 50 and 70 by varying the tube thickness. The increase in the  $D/t$  ratio decreases the ultimate loads of the columns as illustrated in Figure 14. The column ultimate loads are reduced by 12.3% and 16.7%, respectively by increasing the  $D/t$  ratio from 30 to 50 and 70. This can be attributed to the fact that increasing the  $D/t$  ratio decreases the cross-sectional area of the circular steel tube and the confinement to the core concrete.

### 7.2 | Influences of the width-to-diameter ( $B/D$ ) ratio

The  $B/D$  ratio of the column was changed from 1.2 to 1.4 and 1.6 by increasing the width of the outer section. The results given in Figure 15 demonstrate that increasing the  $B/D$  ratio increases the cross-sectional area of the outer concrete which significantly improves the ultimate loads of the columns. When the  $B/D$  ratio is changed from 1.2 to 1.6, the column ultimate load increases by 65.3%. However, the ductility of the columns reduces as the  $B/D$  ratio of the columns increases as shown in Figure 15.

### 7.3 | Influences of the concrete strength

The sensitivity of the performance of CECFST columns to the concrete strength was studied by changing the strength of concrete from 30 to 50 MPa and 70 MPa. The  $P-\epsilon$  curves of the columns with varying concrete strengths are presented in Figure 16. It is discovered that

TABLE 4 Comparisons of the ultimate strengths of CECFST columns

Specimen	Inner tube			Yield			Longitudinal bar			Stirrup			$P_{u, \text{num}}$ (kN)	$P_{u, \text{test}}$ (kN)	$f_{\text{ys}}$ (MPa)	Dia. ( $\phi_p$ )-spacing (mm)	$P_{u, \text{num}}$ $P_{u, \text{test}}$	References
	$L$ (mm)	$B \times B$ (mm)	Dimension $D \times t$ (mm)	$f_{\text{sy}}$ (MPa)	strength, $f_{\text{co}}$ (MPa)	$f'_{\text{ci}}$ (MPa)	$f'_{\text{ci}}$ (MPa)	$f_{\text{yr}}$ (MPa)	$f_{\text{yr}}$ (MPa)	$f_{\text{ys}}$ (MPa)	$f_{\text{ys}}$ (MPa)	$f_{\text{ys}}$ (MPa)						
R1-1	450	150 × 150	60 × 1.98	325	47.2	47.2	47.2	47.2	47.2	380	380	380	1183	1270	376	6.5@100	0.93	Liu <sup>39</sup>
R1-2	450	150 × 150	60 × 1.98	325	47.2	47.2	47.2	47.2	47.2	380	380	380	1183	1252	376	6.5@100	0.94	
R2-1	450	150 × 150	60 × 1.98	325	64.1	64.1	64.1	64.1	64.1	380	380	380	1334	1303	376	6.5@100	1.02	
R2-2	450	150 × 150	60 × 1.98	325	64.1	64.1	64.1	64.1	64.1	380	380	380	1334	1274	376	6.5@100	1.05	
CDCFT1-1	950	250 × 250	165 × 2.85	340	33.3	33.3	33.3	33.3	33.3	362.3	362.3	362.3	2498	2663	413	6@50	0.94	Nie et al. <sup>40</sup>
CDCFT1-2	950	250 × 250	165 × 2.85	340	35.2	35.2	35.2	35.2	35.2	362.3	362.3	362.3	2590	2652	413	6@50	0.98	
CDCFT1-3	950	250 × 250	165 × 2.85	340	32.5	32.5	32.5	32.5	32.5	362.3	362.3	362.3	2452	2633	413	6@50	0.93	
CDCFT2-1	980	300 × 300	219 × 3.52	309	32.1	32.1	32.1	32.1	32.1	362.3	362.3	362.3	3391	3451	413	6@50	0.98	
CDCFT2-2	980	300 × 300	219 × 3.52	309	33.5	33.5	33.5	33.5	33.5	362.3	362.3	362.3	3524	3515	413	6@50	1.00	
CDCFT2-3	980	300 × 300	219 × 3.52	309	31.9	31.9	31.9	31.9	31.9	362.3	362.3	362.3	3384	3615	413	6@50	0.94	
A1-1	600	200 × 200	127 × 1.5	270	55.9	55.9	55.9	55.9	55.9	391	391	391	2253	2510	316	6@100	0.90	Chen <sup>37</sup>
A1-2	600	200 × 200	127 × 1.5	270	55.9	55.9	55.9	55.9	55.9	391	391	391	2253	2447	316	6@100	0.92	
B1-1	600	200 × 200	129 × 2.5	270	58.5	58.5	58.5	58.5	58.5	391	391	391	2460	2850	316	6@100	0.86	
B1-2	600	200 × 200	129 × 2.5	270	58.5	58.5	58.5	58.5	58.5	391	391	391	2460	2992	316	6@100	0.82	
C1-1	600	200 × 200	131 × 3.5	270	57.2	57.2	57.2	57.2	57.2	391	391	391	2426	2594	316	6@100	0.94	
C1-2	600	200 × 200	131 × 3.5	270	57.2	57.2	57.2	57.2	57.2	391	391	391	2426	2761	316	6@100	0.88	
D1-1	600	200 × 200	133 × 4.5	270	56.2	56.2	56.2	56.2	56.2	391	391	391	2602	2842	316	6@100	0.92	
D1-2	600	200 × 200	133 × 4.5	270	56.2	56.2	56.2	56.2	56.2	391	391	391	2602	2906	316	6@100	0.90	
CSTRC1	1200	400 × 400	140 × 6	348	27.1	27.1	27.1	27.1	27.1	356.7	356.7	356.7	5375	5384	340	8@100	1.00	Liu et al. <sup>41</sup>
CSTRC2	1200	400 × 400	140 × 6	348	36.5	36.5	36.5	36.5	36.5	356.7	356.7	356.7	7154	7219	340	8@100	0.99	
CSTRC4	1200	400 × 400	168 × 8	352	27.1	27.1	27.1	27.1	27.1	356.7	356.7	356.7	5878	5738	340	8@100	1.02	
CSTRC5	1200	400 × 400	168 × 8	352	36.5	36.5	36.5	36.5	36.5	356.7	356.7	356.7	7695	7899	340	8@100	0.97	
CSTRC6	1200	400 × 400	180 × 10	333	36.5	36.5	36.5	36.5	36.5	356.7	356.7	356.7	7881	7910	340	8@100	1.00	
CSTRC7	1200	400 × 400	180 × 10	333	36.5	36.5	36.5	36.5	36.5	356.7	356.7	356.7	8112	8458	340	8@100	0.96	
CEC1-1	1200	400 × 400	320 × 6	359	28.9	28.9	28.9	28.9	28.9	432.0	432.0	432.0	7428	7437	483	8@150	1.00	This study
CEC1-2	1200	400 × 400	320 × 10	347	28.9	28.9	28.9	28.9	28.9	432.0	432.0	432.0	9366	9468	483	8@150	0.99	
CEC2-1	1500	500 × 500	400 × 8	308	28.9	28.9	28.9	28.9	28.9	470.1	470.1	470.1	11,777	12,578	483	8@120	0.94	
CEC2-2	1500	500 × 500	400 × 12	372	28.9	28.9	28.9	28.9	28.9	470.1	470.1	470.1	15,112	15,021	483	8@120	1.01	

TABLE 4 (Continued)

	Inner tube			Longitudinal bar				Stirrup						
	$L$ (mm)	$B \times B$ (mm)	Dimension $D \times t$ (mm)	Yield strength, $f_{sy}$ (MPa)	$f'_{co}$ (MPa)	$f'_{ci}$ (MPa)	$no \times dia. (\phi_l)$ (mm)	$f_{yr}$ (MPa)	Dia. $(\phi_p)$ -spacing (mm)					
Specimen										$f_{yrs}$ (MPa)	$P_{u,test}$ (kN)	$P_{u,num}$ (kN)	$\frac{P_{u,num}}{P_{u,test}}$	References
CEC3-1	1800	600 × 600	500 × 10	347	28.9	39.5	12Φ18	442.7	10@200	435	18,318	17,731	0.97	
CEC3-2	1800	600 × 600	500 × 16	384	28.9	39.5	12Φ18	442.7	10@200	435	22,880	23,008	1.01	
Mean													0.96	
SD													0.05	
Coefficient of Variation (CoV)													0.05	

the column ultimate load increases due to the increase in the concrete strength. However, using high-strength concrete reduces the ductility of the columns. The ultimate load increases by 80.7% by changing the strength of concrete from 30 to 70 MPa. Figure 17 also presents the influences of the strengths of the core concrete and outer concrete on the  $P - \epsilon$  curves of the columns. When the strength of the core concrete was changed from 30 to 70 MPa, the strength of outer concrete remained the same as 50 MPa. Similarly, the strength of the core concrete remained constant as 50 MPa when the strength of the outer concrete was varied. It is seen that the influences of the outer concrete on the ultimate loads and ductility of the columns are more pronounced than that of the core concrete. The percentage increase in the ultimate load is 44% for the outer concrete while it is 23.8% for the increase of the core concrete from 30 to 70 MPa.

#### 7.4 | Influences of the steel yield strength

The effects of the steel yield strength of the steel tube and the longitudinal rebars of CECFST columns were investigated by changing their yield stress. The  $P - \epsilon$  curves of the columns made of steel with varying yield stress are provided in Figure 18. The column ultimate load is increased by 12.3% by changing the yield strength of the inner steel tube from 250 to 450 MPa. However, the ductility of the columns is found to be remained unchanged for the change of the yield stress. On the contrary, the increase in the ultimate strength is only 2% when the yield stress of the longitudinal bars increases from 400 to 600 MPa.

#### 7.5 | Influences of the longitudinal bar ratio ( $\alpha_l$ )

To investigate the sensitivities of the performance of short CECFST columns to  $\alpha_l$  ratio, the diameter of the longitudinal bar was changed to vary the  $\alpha_l$  ratio from 1% to 2% and 3%. The influences of  $\alpha_l$  ratio on the  $P - \epsilon$  curves of the columns are shown in Figure 19. The column ultimate strength has an increase of 7.3% when  $\alpha_l$  ratio increases from 1% to 3%. The influence of  $\alpha_l$  ratio on the ductility of the columns is also found to be insignificant as can be seen from Figure 19.

#### 7.6 | Influences of the spacing of stirrups

The significance of stirrup spacing on the behavior of short CECFST columns was investigated by varying the

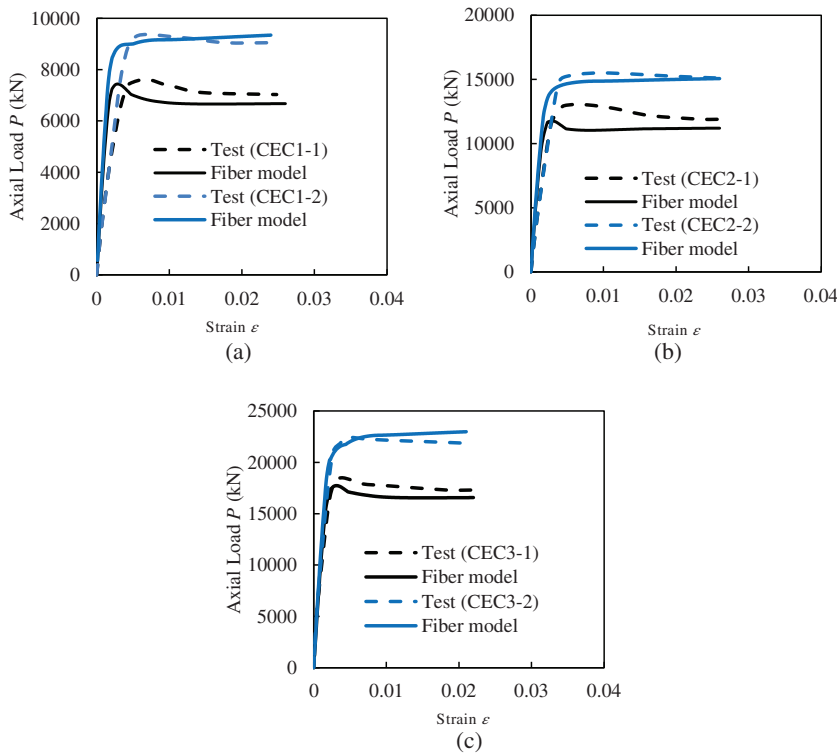


FIGURE 12 Comparisons of predicted  $P-\epsilon$  curves of CECFST columns with the test results reported in this study

spacing from 100 to 200 mm and 300 mm. The  $P-\epsilon$  curves of the columns are presented in Figure 20, which indicates that the influence of spacing is more pronounced on the ductility of the column rather than on its ultimate strength. When the spacing decreases to 100 mm from 300 mm, the column ultimate load improves only about 1.8%. Furthermore, the column with a stirrup space of 100 mm has better ductility than other columns. This is because decreasing the spacing of stirrups improves the confinement to the outer concrete which results in an improvement in the column ductility.

## 8 | DESIGN MODELS

### 8.1 | Codified methods

Design specifications given by CECS 188-2019,<sup>60</sup> Eurocode 4,<sup>57</sup> ACI 318-19,<sup>58</sup> and AIJ<sup>59</sup> were employed to calculate the ultimate strengths of concrete-encased CFST columns loaded axially and compared against the test results to evaluate their accuracy. Table 5 summarizes the codified design formulas that are utilized to compute the ultimate compressive strengths of short columns. From the comparisons presented in Table 6, it is observed that existing codes cannot accurately yield the ultimate compressive loads. Among the existing codes,

AIJ provides better estimations than others while Eurocode 4 significantly overestimates the ultimate loads of such columns. However, AIJ significantly underestimates the ultimate strengths of the tested columns reported by Chen.<sup>37</sup>

### 8.2 | Proposed design model

Simple design formulas for estimating the ultimate loads of axially loaded CECFST columns are proposed as follows:

$$P_{\text{prop}} = P_{\text{rc}} + P_{\text{CFST}} \quad (20)$$

$$P_{\text{rc}} = A_l f_{\text{yr}} + A_{\text{co}} f'_{\text{co}} \quad (21)$$

$$P_{\text{CFST}} = A_s f_{\text{sy}} + A_{\text{ci}} f'_{\text{cc}} \quad (22)$$

where  $P_{\text{rc}}$  and  $P_{\text{CFST}}$  are the axial bearing capacities of reinforced section and inner CFST columns, respectively;  $A$  is the cross-sectional area, subscript  $co$ ,  $ci$ ,  $l$ , and  $s$  refer to the outer concrete, core concrete, longitudinal bar, and steel tube, respectively;  $f_{\text{sy}}$  and  $f_{\text{yr}}$  are the steel yield stresses of steel tube and longitudinal rebar, respectively;  $f'_{\text{cc}}$  refers to the compressive strengths of confined concrete calculated using Equation (3).



**FIGURE 13** Comparisons of predicted  $P - \epsilon$  curves of CECFST columns with the test results reported by other researchers

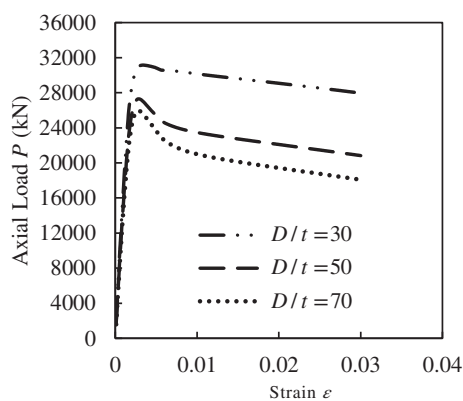
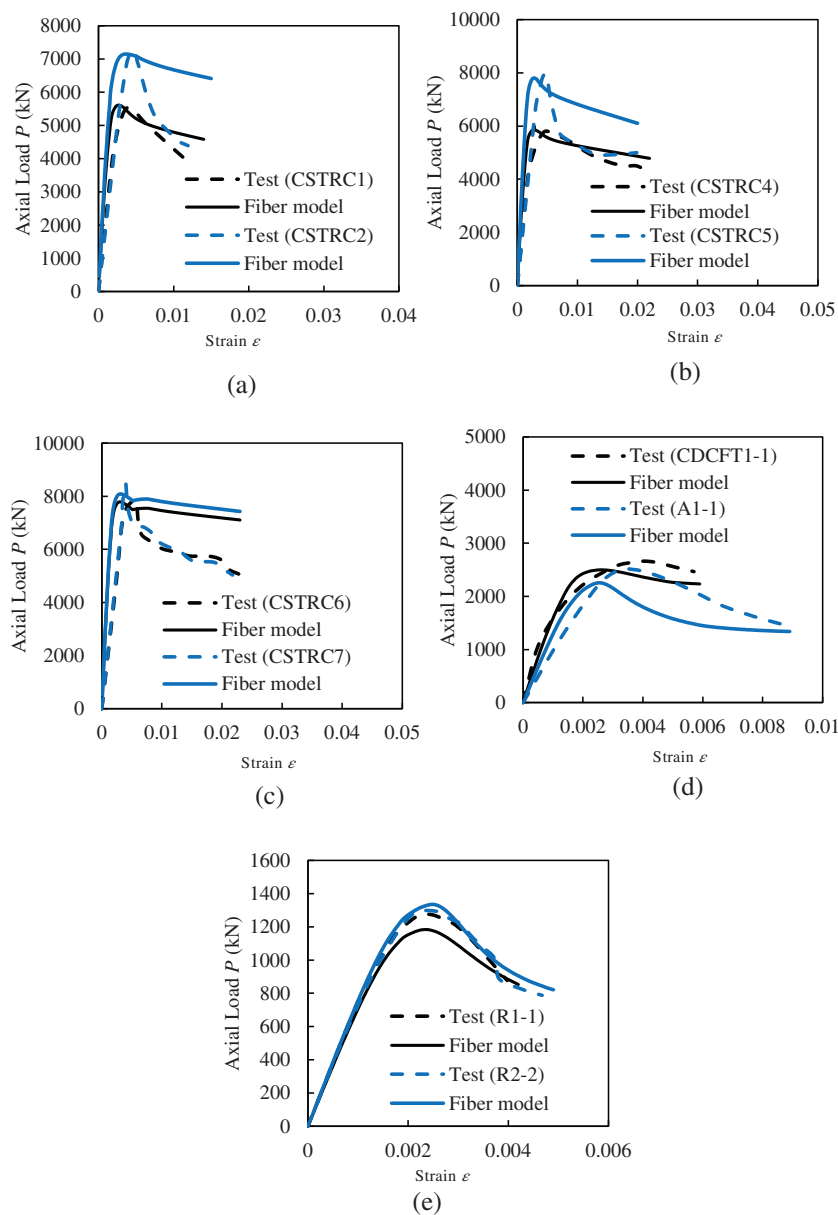


**FIGURE 14** Influences of  $D/t$  ratio on the  $P - \epsilon$  curves

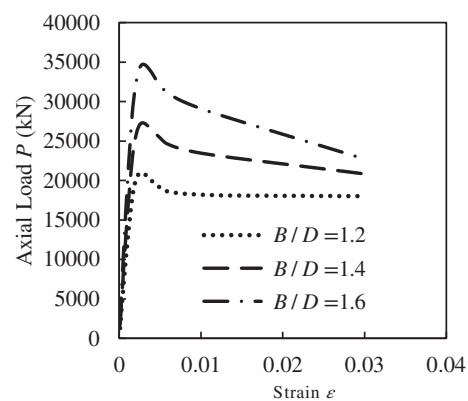


**FIGURE 15** Influences of  $B/D$  ratio on the  $P - \epsilon$  curves

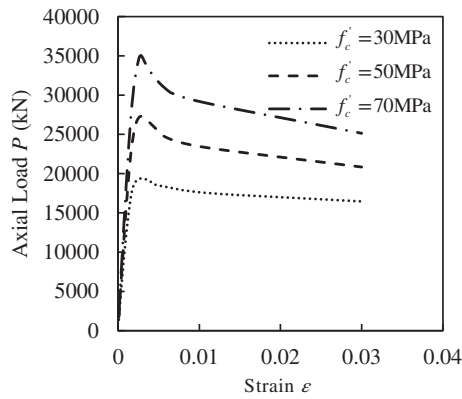


**FIGURE 16** Influences of concrete strength on the  $P-\varepsilon$  curves

The accuracy of the proposed design model is validated by comparing the design ultimate strengths against the test results and presented in Table 5. The proposed design model is found to provide reasonable estimations of the ultimate loads of CECFST columns. The mean predicted-to-experimental ultimate load value of 0.99 with a corresponding SD of 0.08 was obtained.

## 9 | CONCLUSIONS

This article has presented an experimental program carried out on axially loaded square concrete-encased concrete-filled large-diameter steel tubular short columns. A mathematical model has also been developed based on the theory of the fiber analysis method for the computer simulation of CECFST columns. The model has considered the concrete confinement caused by the inner steel tube and stirrups and the inelastic buckling of longitudinal rebars. The accuracy of the computational program has been verified against the test data and used to perform a detailed parameter study. The accuracy of the codified design models has been investigated and a simple design formula has been suggested to determine the ultimate compressive strengths of such columns loaded axially.

The following conclusions are drawn from this study:

1. The common failure modes of the tested CECFST short columns loaded concentrically were the concrete crushing and spalling of the outer concrete, associated with the deformation of stirrups and longitudinal

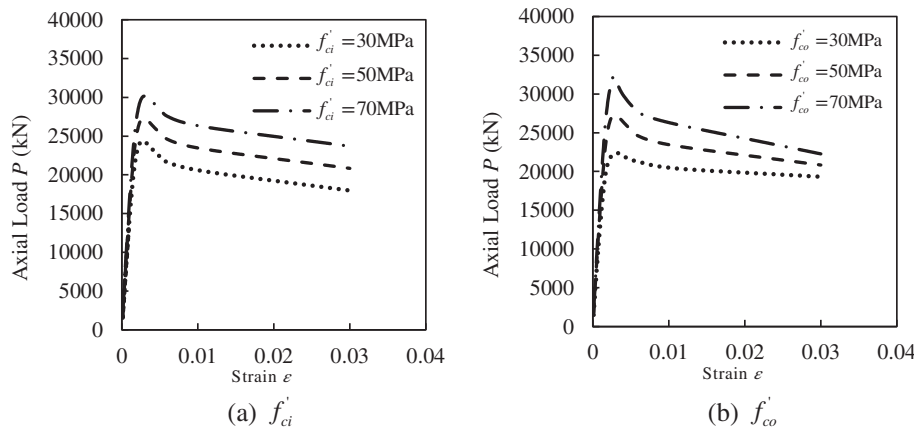


**FIGURE 17** Influences of the strength of the core concrete and outer concrete on the  $P-\varepsilon$  curves

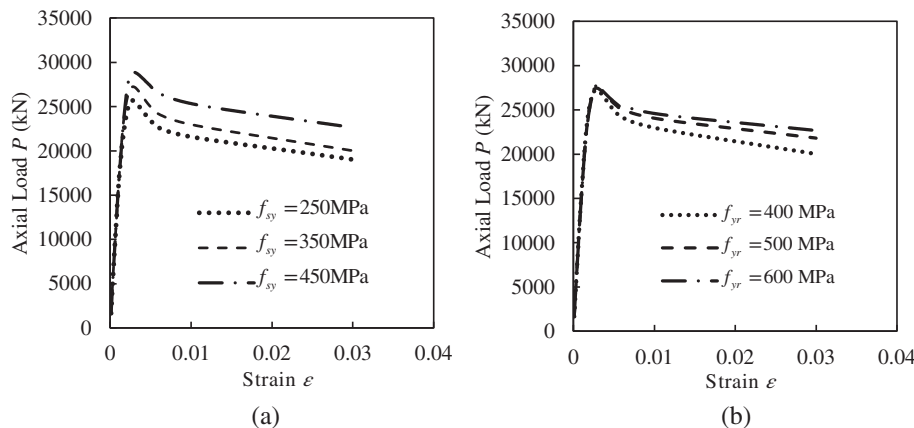


**FIGURE 18** Influences of the steel yield stress of the steel tube and longitudinal bars on the  $P-\varepsilon$  curves: (a) steel tube and (b) longitudinal bar

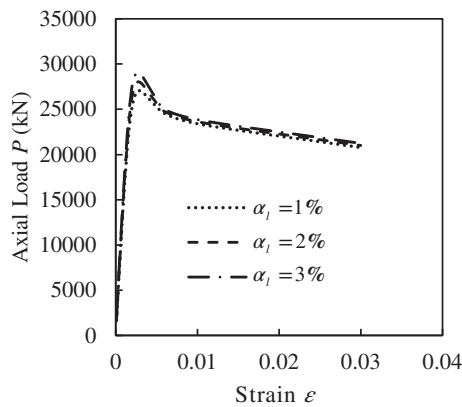


FIGURE 19 Influences of longitudinal bar ratio on the  $P-\epsilon$  curves

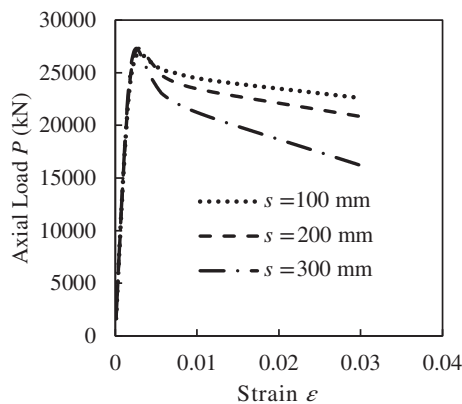


FIGURE 20 Influences of stirrup spacing on the  $P-\epsilon$  curves

TABLE 5 Design formulas for predicting the ultimate axial strengths of CECFST columns

Design models	Design equations
Eurocode 4	<p>Inner circular CFST column:</p> $P_{CFST} = \eta_a A_s f_{sy} + A_{ci} f'_{ci} \left( 1 + \eta_c \frac{t}{D} \frac{f_{sy}}{f'_{ci}} \right)$ $\eta_a = 0.25 (3 + 2\lambda) \quad (\eta_a \leq 1.0)$ $\eta_c = 4.9 - 18.5\lambda + 17\lambda^2 \quad (\eta_c > 0)$ $-\lambda = \sqrt{\frac{N_{pl,Rk}}{N_{cr}}}$ <p>Outer section:</p> $P_{rc} = A_t f_{yr} + A_{co} f'_{co}$ <p>Concrete-encased CFST columns</p> $P_{u,EC4} = P_{rc} + P_{CFST}$
ACI 318-19	$P_{u,ACI} = A_t f_{yr} + 0.85 A_{co} f'_{co} + A_s f_{sy} + 0.85 A_{ci} f'_{ci}$
CECS 188-2019	$P_{u,CECS} = 0.9 (P_{rc} + P_{CFST})$ $P_{rc} = A_t f_{yr} + A_{co} f'_{co}$ $P_{CFST} = \begin{cases} 0.9 f_{ck} A_{ci} (1 + \alpha \theta) & \text{for } \theta \leq 1/(\alpha - 1)^2 \\ 0.9 f_{ck} A_{ci} (1 + \sqrt{\theta} + \theta) & \text{for } 1/(\alpha - 1)^2 < \theta \leq 2.5 \end{cases}$ $\theta = \frac{A_s f_{sy}}{A_{ci} f_{ck}}$ $f_{ck} = 0.67 f_{cu}$ $\alpha = \begin{cases} 2 & \text{for } f_{cu} \leq 50 \text{ MPa} \\ 1.8 & \text{for } 50 < f_{cu} \leq 100 \text{ MPa} \end{cases}$
AIJ	$P_{u,AIJ} = A_t f_{yr} + A_{co} f'_{co} + A_s f_{sy} + A_{ci} f'_{ci}$

bars. The outer concrete effectively prevented the inner steel tube from local buckling.

- The encased CFST columns improved the ultimate strength of the CECFST columns. The increase in the ultimate strength calculated varied from 6% to 12% when compared with the ultimate load of the CECFST columns calculated employing the superposition method.
- The stub columns failed in a ductile manner where the residual strengths of the columns were still at 85–95% of their peak loads.
- Increasing the steel tube thickness remarkably improved their ultimate strengths. This is due to the improvement of the composite action of the steel and concrete of the inner CFST columns. The rate of increase in the compressive strength of the core concrete of the CFST column was found to be higher for the column with a smaller local slenderness ratio.
- Parameter study shows that the strength of the outer concrete and spacing of stirrups have a significant effect on the ductility of CECFST columns.
- The increase in the longitudinal bar ratio increases the ultimate strength of the columns, however, the longitudinal bar ratio has insignificant effects on the ductility of the columns.
- The existing design models cannot provide accurate estimations of the ultimate strengths of CECFST columns loaded axially. Among all, Eurocode 4 provides a significant overestimation of the ultimate strength of CECFST columns. Although AIJ provides better

TABLE 6 Comparisons of the design ultimate strengths of CECFST columns using various design models

Specimen	$P_{u,test}$ (kN)	$P_{u,EC4}$ (kN)	$\frac{P_{u,EC4}}{P_{u,test}}$	$P_{u,ACI}$ (kN)	$\frac{P_{u,ACI}}{P_{u,test}}$	$P_{u,AIJ}$ (kN)	$\frac{P_{u,AIJ}}{P_{u,test}}$	$P_{u,CECS}$ (kN)	$\frac{P_{u,CECS}}{P_{u,test}}$	$P_{u,prop}$ (kN)	$\frac{P_{u,prop}}{P_{u,test}}$	References
R1-1	1270	1188	0.94	994	0.78	1122	0.88	941	0.74	1178	0.93	Liu <sup>39</sup>
R1-2	1252	1188	0.95	994	0.79	1122	0.90	941	0.75	1178	0.94	
R2-1	1303	1451	1.11	1218	0.93	1385	1.06	1107	0.85	1441	1.11	
R2-2	1274	1451	1.14	1218	0.96	1385	1.09	1107	0.87	1441	1.13	
CDCFT1-1	2663	2776	1.04	2209	0.83	2483	0.93	2326	0.87	2554	0.96	Nie et al. <sup>40</sup>
CDCFT1-2	2652	2876	1.08	2294	0.86	2582	0.97	2391	0.90	2651	1.00	
CDCFT1-3	2633	2732	1.04	2171	0.82	2438	0.93	2297	0.87	2510	0.95	
CDCFT2-1	3451	3906	1.13	3082	0.89	3467	1.00	3275	0.95	3531	1.02	
CDCFT2-2	3515	4023	1.14	3181	0.90	3584	1.02	3351	0.95	3642	1.04	
CDCFT2-3	3615	3892	1.08	3070	0.85	3453	0.96	3265	0.90	3517	0.97	
A1-1	2510	2304	0.92	1918	0.76	2207	0.88	1640	0.65	2226	0.89	Chen <sup>37</sup>
A1-2	2447	2304	0.94	1918	0.78	2207	0.90	1672	0.68	2226	0.91	
B1-1	2850	2539	0.89	2082	0.73	2381	0.84	1904	0.67	2415	0.85	
B1-2	2992	2539	0.85	2082	0.70	2381	0.80	1904	0.64	2415	0.81	
C1-1	2594	2644	1.02	2137	0.82	2425	0.93	2069	0.80	2622	1.01	
C1-2	2761	2644	0.96	2137	0.77	2425	0.88	2069	0.75	2622	0.95	
D1-1	2842	2755	0.97	2199	0.77	2479	0.87	2252	0.79	2701	0.95	
D1-2	2906	2755	0.95	2199	0.76	2479	0.85	2252	0.77	2701	0.93	
CSTRC1	5384	6082	1.13	5022	0.93	5601	1.04	5021	0.93	5827	1.08	Liu et al. <sup>41</sup>
CSTRC2	7219	7512	1.04	6237	0.86	7031	0.97	6097	0.84	7333	1.02	
CSTRC4	5738	6859	1.20	5524	0.96	6097	1.06	5820	1.01	6417	1.12	
CSTRC5	7899	8311	1.05	6757	0.86	7549	0.96	6980	0.88	7976	1.01	
CSTRC6	7910	8677	1.10	6978	0.88	7744	0.98	7433	0.94	8184	1.03	
CSTRC7	8458	8813	1.04	7093	0.84	7879	0.93	7618	0.90	8355	0.99	
CEC1-1	7437	8897	1.20	6900	0.93	7639	1.03	7779	1.05	7684	1.03	This study
CEC1-2	9468	10,665	1.13	8026	0.85	8743	0.92	9711	1.03	9817	1.04	
CEC2-1	12,578	13,710	1.09	10,758	0.86	11,921	0.95	11,936	0.95	11,789	0.94	
CEC2-2	15,021	17,247	1.15	13,005	0.87	14,139	0.94	15,597	1.04	15,727	1.05	
CEC3-1	18,318	20,945	1.14	16,130	0.88	17,796	0.97	18,576	1.01	17,542	0.96	
CEC3-2	22,880	26,744	1.17	19,831	0.87	21,443	0.94	24,415	1.07	23,913	1.05	
Mean			1.05		0.84		0.95		0.87		0.99	
SD			0.10		0.07		0.07		0.12		0.08	
CoV			0.09		0.08		0.07		0.14		0.08	

estimations, it significantly underestimated the ultimate strengths of some CECFST tested columns.

- The proposed design model in this study considers the confinement effects of the inner steel tube and can predict the ultimate loads with reasonable accuracy.

The investigations into the behavior of large-diameter CECFST columns presented in this study provide useful insight into the understanding of their axial performance under concentric loading. Furthermore, the tested

columns reported in this study covers a wide range of local slenderness ratio of inner steel tube of CECFST columns which are within the slenderness limit specified by existing design codes. The excellent axial performance of CECFST columns observed in this study will provide confidence to the structural engineers in adopting such a column in wider applications in practice. However, the findings of this study demonstrate that the existing codified design models can not accurately predict the ultimate strengths of CFCFST columns. Therefore, new



design guidelines should be developed to facilitate the application of such a column in practice. Furthermore, future studies should investigate the performance of CECFST slender columns subjected to eccentric loading and develop design models.

## ACKNOWLEDGMENT

Open access publishing facilitated by University of Wollongong, as part of the Wiley - University of Wollongong agreement via the Council of Australian University Librarians.

## DATA AVAILABILITY STATEMENT


The data that support the findings of this study are available from the corresponding author upon reasonable request.

## ORCID

Junchang Ci  <https://orcid.org/0000-0001-9717-9702>

Lingxu Kong  <https://orcid.org/0000-0001-7818-9008>

Mizan Ahmed  <https://orcid.org/0000-0001-5499-3181>

Qing Quan Liang  <https://orcid.org/0000-0003-0333-2265>

Ahmed Hamoda  <https://orcid.org/0000-0001-5952-5272>

Shicai Chen  <https://orcid.org/0000-0002-0135-0040>

Chunyu Wu  <https://orcid.org/0000-0002-3253-9153>

## REFERENCES

- Naghipour M, Ahmadi M, Nematzadeh M. Effect of concrete confinement level on load-bearing capacity of steel-reinforced concrete (SRC) columns under eccentric loading: experiment and FEA model. *Structure*. 2022;35:202–13.
- Ahmed M, Ci J, Yan X-F, Lin S, Chen S. Numerical modeling of axially loaded circular concrete-filled double-skin steel tubular short columns incorporating a new concrete confinement model. *Structure*. 2021;30:611–27.
- Ahmed M, Tran V-L, Ci J, Yan X-F, Wang F. Computational analysis of axially loaded thin-walled rectangular concrete-filled stainless steel tubular short columns incorporating local buckling effects. *Structure*. 2021;34:4652–68.
- Nematzadeh M, Memarzadeh A, Karimi A. Post-fire elastic modulus of rubberized fiber-reinforced concrete-filled steel tubular stub columns: experimental and theoretical study. *J Constr Steel Res*. 2020;175:106310.
- Memarzadeh A, Nematzadeh M. Axial compressive performance of steel reinforced fibrous concrete composite stub columns: experimental and theoretical study. *Structure*. 2021;34:2455–75.
- Nematzadeh M, Karimi A, Gholampour A. Pre-and post-heating behavior of concrete-filled steel tube stub columns containing steel fiber and tire rubber. *Structure*. 2020;27:2346–64.
- Ahmed M, Liang QQ, Hamoda A, Arashpour M. Behavior and design of thin-walled double-skin concrete-filled rectangular steel tubular short and slender columns with external stainless-steel tube incorporating local buckling effects. *Thin-Walled Struct*. 2022;170:108552.
- Kong LX. Study on the axial compression behavior of CFST composite columns with large diameter width ratio. 2020, Beijing University of Technology, Beijing, China, Master Thesis. (in Chinese)
- Han L-H, An Y-F. Performance of concrete-encased CFST stub columns under axial compression. *J Constr Steel Res*. 2014;93:62–76.
- Fx D, Yf C, Yj Y, Lp W, Zw Y. Composite action of rectangular concrete-filled steel tube columns under lateral shear force. *Struct. Con*. 2020;22:1–15.
- Farajpourbonab E. Development of a new steel section for reinforcing of steel-reinforced concrete-filled steel tubular columns. *Struct. Con*. 2019;20(2):689–706.
- Gupta PK, Ahuja AK, Khaudhair ZA. Modelling, verification and investigation of behaviour of circular CFST columns. *Struct. Con*. 2014;15(3):340–9.
- Li J, Deng Z, Sun T. Flexural behavior of ultra-high performance concrete filled high-strength steel tube. *Struct. Con*. 2021;22:1–20.
- Sakino K, Nakahara H, Morino S, Nishiyama I. Behavior of centrally loaded concrete-filled steel-tube short columns. *J. Struct. Eng*. 2004;130(2):180–8.
- Han LH. Tests on stub columns of concrete-filled RHS sections. *J Constr Steel Res*. 2002;58(3):353–72.
- Uy B. Strength of concrete filled steel box columns incorporating local buckling. *J. Struct. Eng*. 2000;126(3):341–52.
- Tao Z, Wang Z-B, Yu Q. Finite element modelling of concrete-filled steel stub columns under axial compression. *J Constr Steel Res*. 2013;89:121–31.
- Xiong MX, Xiong DX, Liew JYR. Axial performance of short concrete filled steel tubes with high-and ultra-high-strength materials. *Eng Struct*. 2017;136:494–510.
- Yu F, Fang Y, Zhang Y, Xu L, Bai R. Mechanical behavior of self-stressing steel slag aggregate concrete filled steel tubular stub columns. *Struct Con*. 2020;21(4):1597–611.
- Ahmed M, Liang QQ, Patel VI, Hadi MNS. Experimental and numerical studies of square concrete-filled double steel tubular short columns under eccentric loading. *Eng Struct*. 2019;197:109419.
- Ahmed M, Liang QQ, Patel VI, Hadi MNS. Experimental and numerical investigations of eccentrically loaded rectangular concrete-filled double steel tubular columns. *J Constr Steel Res*. 2020;167:105949.
- Ahmed M, Ci J, Yan X-F, Chen S. Nonlinear analysis of elliptical concrete-filled stainless steel tubular short columns under axial compression. *Structure*. 2021;32:1374–85.
- Ahmed M, Liang QQ. Computational simulation of elliptical concrete-filled steel tubular short columns including new confinement model. *J Constr Steel Res*. 2020;174:106294.
- Lam D, Gardner L, Burdett M. Behaviour of axially loaded concrete filled stainless steel elliptical stub columns. *Adv Struct Eng*. 2010;13(3):493–500.
- Hassanein MF, Patel VI, Bock M. Behaviour and design of hexagonal concrete-filled steel tubular short columns under axial compression. *Eng Struct*. 2017;153:732–48.
- Ahmed M, Liang QQ. Numerical analysis of concentrically loaded hexagonal concrete-filled steel tubular short columns incorporating concrete confinement. *Adv Struct Eng*. 2021;13694332211004111:111405.
- Ding F-X, Li Z, Cheng S, Yu Z-W. Composite action of hexagonal concrete-filled steel tubular stub columns under axial loading. *Thin-Walled Struct*. 2016;107:502–13.

28. Xu W, Han L-H, Li W. Performance of hexagonal CFST members under axial compression and bending. *J Constr Steel Res.* 2016;123:162–75.
29. Ahmed M, Liang QQ. Numerical analysis of thin-walled round-ended concrete-filled steel tubular short columns including local buckling effects. *Structure.* 2020;28:181–96.
30. Hassanein MF, Patel VI. Round-ended rectangular concrete-filled steel tubular short columns: FE investigation under axial compression. *J Constr Steel Res.* 2018;140:222–36.
31. Shen Q, Wang J, Wang W, Wang Z. Performance and design of eccentrically-loaded concrete-filled round-ended elliptical hollow section stub columns. *J Constr Steel Res.* 2018;150:99–114.
32. Wang Z, Chen J, Xie E, Lin S. Behavior of concrete-filled round-ended steel tubular stub columns under axial compression. *J. Build. Struct.* 2014;35(7):123–30. (Chinese).
33. Ahmed M, Liang QQ. Numerical modeling of octagonal concrete-filled steel tubular short columns accounting for confinement effects. *Eng Struct.* 2020;226:111405.
34. Ding F-X, Li Z, Cheng S, Yu Z-W. Composite action of octagonal concrete-filled steel tubular stub columns under axial loading. *Thin-Walled Struct.* 2016;107:453–61.
35. Hassanein MF, Patel VI, Elchalakani M, Thai H-T. Finite element analysis of large diameter high strength octagonal CFST short columns. *Thin-Walled Struct.* 2018;123:467–82.
36. Zhu J-Y, Chan T-M. Experimental investigation on octagonal concrete filled steel stub columns under uniaxial compression. *J Constr Steel Res.* 2018;147:457–67.
37. Chen ZY. Study of the method for design and calculation of HSC columns reinforced with concrete filled steel tube. 2002, Dalian University of Technology, Dalian, China, PhD Thesis. (in Chinese)
38. Zhen KH. Study on mechanical properties of concrete-filled steel tube composite columns. 2009, Tsinghua University, Beijing, China, PhD Thesis. (in Chinese)
39. Liu LY. Study on behavior of a new concrete-filled steel tube reinforced concrete column under axial compression. 2013, Fuzhou university, Fuzhou, China, Master Thesis. (in Chinese)
40. Nie JG, Bai Y, Cai CS. New connection system for confined concrete columns and beams. I: experimental study. *J Struct Eng.* 2008;134:1787–99.
41. Liu Y, Guo ZX, Jia LP, Chen QM. Experimental study on axial compression performance and design method of core steel tube reinforced concrete short columns. *J. Build. Struct.* 2015;36(12):135–42. (in Chinese).
42. Ji X, Kang H, Chen X, Qian J. Seismic behavior and strength capacity of steel tube-reinforced concrete composite columns. *Earth Eng Struct Dyn.* 2014;43(4):487–505.
43. Han L-H, Liao F-Y, Tao Z, Hong Z. Performance of concrete filled steel tube reinforced concrete columns subjected to cyclic bending. *J Constr Steel Res.* 2009;65(8–9):1607–16.
44. Ma Y-X, Zhao O, Tan KH. Experimental and numerical studies of concrete-encased concrete-filled steel tube stub columns under uniaxial and biaxial eccentric compression. *Eng Struct.* 2021;232:111796.
45. Zhou K, Han L-H. Experimental and numerical study of temperature developments of composite joints between concrete-encased concrete-filled steel tube columns and reinforced concrete beams. *Fire Safety J.* 2020;116:103187.
46. Guo QQ, Zhao YX, Li Q, Shang K. Experimental study on eccentric compressive property of steel tube-reinforced concrete columns. *J Build Struct.* 2013;34(12):103–11.
47. Guo QQ, Li Q, Zhang PY, Hu JT. Calculation for bearing capacity of steel tube-reinforced concrete columns under eccentric compression. *China Civil Eng J.* 2014;47(5):56–63. (in Chinese).
48. An Y-F, Han L-H, Zhao X-L. Experimental behaviour of box concrete-encased CFST eccentrically loaded column. *Mag Conc Res.* 2013;65(20):1219–35.
49. An Y-F, Han L-H. Behaviour of concrete-encased CFST columns under combined compression and bending. *J Constr Steel Res.* 2014;101:314–30.
50. Liang QQ. Performance-based analysis of concrete-filled steel tubular beam-columns, part I: theory and algorithms. *J Constr Steel Res.* 2009;65(2):363–72.
51. Patel VI, Liang QQ, Hadi MNS. Numerical simulations of circular high strength concrete-filled aluminum tubular short columns incorporating new concrete confinement model. *Thin-Walled Struct.* 2020;147:106492.
52. Lai ZC, Varma AH. Effective stress-strain relationships for analysis of noncompact and slender filled composite (CFT) members. *Eng Struct.* 2016;124:457–72.
53. Tao Z, Han L-H. Behaviour of concrete-filled double skin rectangular steel tubular beam-columns. *J Constr Steel Res.* 2006;62(7):631–46.
54. Tao Z, Han LH, Zhao XL. Behaviour of concrete-filled double skin (CHS inner and CHS outer) steel tubular stub columns and beam-columns. *J Constr Steel Res.* 2004;60(8):1129–58.
55. Ahmed M, Liang QQ, Patel VI, Hadi MNS. Nonlinear analysis of rectangular concrete-filled double steel tubular short columns incorporating local buckling. *Eng Struct.* 2018;175:13–26.
56. Ahmed M, Liang QQ, Patel VI, Hadi MNS. Numerical analysis of axially loaded circular high strength concrete-filled double steel tubular short columns. *Thin-Walled Struct.* 2019;138:105–16.
57. Eurocode 4: Design of composite steel and concrete structure—part 1-1: general rules and rules for buildings. European Committee for Standardization (CEN) Brussels, Belgium 2004.
58. ACI 318-19. Building code requirements for structure concrete and commentary. Farmington Hills, Michigan, USA. 2019.
59. AIJ Recommendations for design and construction of concrete filled steel tubular structure. Architectural Institute of Japan, Tokyo, Japan 1997.
60. CECS 188. Technical specification for steel tube-reinforced concrete column structure. Beijing, China: China Planning Press; 2019 (in Chinese).
61. AS/NZS 5100. Bridge design. Part 6: steel and composite construction. Australian/New Zealand standard. Sydney, NSW, Australia; 2017.
62. AISC. 360-16. Specification for structural steel buildings. American Institute of Steel Construction. Chicago (IL), USA; 2016.
63. GB/T 228.1-2010. Metallic materials-tensile testing-part 1: method of test at room temperature. China. 2010. (in Chinese)
64. GB/T 50081-2019. Standard for test methods of concrete physical and mechanical properties, China, 2019. (in Chinese)
65. GB/T 50152-2012. Standard for test method of concrete Structure, China, 2012. (in Chinese)
66. L'Hermite R. Idées actuelles sur la technologie du béton. Paris: La Documentation technique du bâtiment et des travaux publics; 1955.

67. Liang QQ. Nonlinear analysis of circular double-skin concrete-filled steel tubular columns under axial compression. *Eng Struct.* 2017;131:639–50.
68. Lin S, Zhao Y-G, Lu Z-H. Fibre beam element models for nonlinear analysis of concentrically loaded circular CFT columns considering the size effect. *Eng Struct.* 2020;210:110400.
69. Mander JB. Seismic design of bridge piers. 1983, Department of Civil Engineering, University of Canterbury, Christchurch, New Zealand, Ph.D. Thesis
70. Chen C-C, Lin N-J. Analytical model for predicting axial capacity and behavior of concrete encased steel composite stub columns. *J Constr Steel Res.* 2006;62(5):424–33.
71. Mander JB, Priestley MJN, Park R. Theoretical stress-strain model for confined concrete. *J. Struct. Eng.* 1988;114(8):1804–26.
72. Liang QQ, Fragomeni S. Nonlinear analysis of circular concrete-filled steel tubular short columns under axial loading. *J Constr Steel Res.* 2009;65(12):2186–96.
73. De Nicolo B, Pani L, Pozzo E. Strain of concrete at peak compressive stress for a wide range of compressive strengths. *Mat Struct.* 1994;27(4):206–10.
74. Tang J, Hino S, Kuroda I, Ohta T. Modeling of stress-strain relationships for steel and concrete in concrete filled circular steel tubular columns. *Steel Constr Eng, JSSC.* 1996;3(11):35–46.
75. Lim JC, Ozbakkaloglu T. Stress-strain model for normal-and light-weight concretes under uniaxial and triaxial compression. *Constr Build Mat.* 2014;71:492–509.
76. El-Tawil S, Deierlein GG. Strength and ductility of concrete encased composite columns. *J. Struct. Eng.* 1999;125(9):1009–19.
77. Zhao X-M, Wu Y-F, Leung AYT. Analyses of plastic hinge regions in reinforced concrete beams under monotonic loading. *Eng Struct.* 2012;34:466–82.
78. Wang N, Shi QX, Zhang W, Zheng GD, Wang HL. A uniaxial compressive model for concrete confined with stirrups. *J Build Mat.* 2019;22(6):933–40. (in Chinese).

## AUTHOR BIOGRAPHIES



**Junchang Ci**, College of Architecture and Civil Engineering, Beijing University of Technology, Beijing, China  
[cjc\\_bjut@163.com](mailto:cjc_bjut@163.com)



**Lingxu Kong**, OCT Northern Investment Co. Ltd., Beijing, China  
[klx1996@163.com](mailto:klx1996@163.com)



**Mizan Ahmed**, School of Civil, Mining, and Environmental Engineering, University of Wollongong, Wollongong, New South Wales, Australia  
[mizan@uow.edu.au](mailto:mizan@uow.edu.au)



**Qing Quan Liang**, College of Engineering and Science, Victoria University, PO Box 14428, Melbourne, VIC 8001, Australia  
[qing.liang@vu.edu.au](mailto:qing.liang@vu.edu.au)



**Ahmed Hamoda**, Department of Civil Engineering, Kafrelsheikh University, Kafrelsheikh, Egypt.  
[ahmed\\_hamoda@eng.kfs.edu.eg](mailto:ahmed_hamoda@eng.kfs.edu.eg)



**Shicai Chen**, College of Architecture and Civil Engineering, Beijing University of Technology, Beijing, China  
[shicaichen@163.com](mailto:shicaichen@163.com)



**Chunyu Wu**, College of Architecture and Civil Engineering, Beijing University of Technology, Beijing, China  
[wuchunyu1213@sina.com](mailto:wuchunyu1213@sina.com)

**How to cite this article:** Ci J, Kong L, Ahmed M, Liang QQ, Hamoda A, Chen S, et al. Experimental and numerical studies of axially loaded square concrete-encased concrete-filled large-diameter steel tubular short columns. *Structural Concrete.* 2022;23:2748–69. <https://doi.org/10.1002/suco.202100466>